Triassic evaporites: a vast reservoir of brines mobilised successively during rifting and thrusting in the Pyrenees

Michel Cathelineau, Marie-Christine Boiron, Hugo Jakomulski

Triassic evaporites: a vast reservoir of brines mobilised successively during rifting and thrusting in the Pyrenees

M. Cathelineau*, M.-C. Boiron and H. Jakomulski

Abstract

Triassic evaporites have a very particular location in the Pyrenees, close to detachment areas between the basement and the sedimentary cover, and constitute enormous chlorine and potentially brine reservoir. During the two successive deformation cycles related successively to the Cretaceous rifting and the convergence during early Cenozoic, brines were expulsed and implied in fault activity, breccia formation and fluid-rock interactions. Fluid inclusions from fault infillings and alpine-style fissures sampled all along the Pyrenean chain have a maximal chlorinity close to that of halite-water equilibrium at temperatures between 250 and 350°C. Mixing of brines with low chlorinity waters formed a series of fluids covering an extensive range of salinities. During syn-rift events, the hotter dilute end-member is likely derived from seawater infiltrated and heated near the exhumed mantle as no emerged areas were present at that time. During convergence and thrusting, brines again predominate and mixing occurred with a colder end-member, probably of meteoric origin, consistent with a significant period of relief formation. Brines played, therefore, an essential role in mass and heat transfer during the whole orogenic cycle in the Pyrenees.

Other pieces of information

Michel Cathelineau
Université de Lorraine, CNRS, CREGU, GeoRessources,54000, Nancy

Marie-Christine Boiron
Université de Lorraine, CNRS, CREGU, GeoRessources, 54000, Nancy

Hugo Jakomulski
Université de Lorraine, CNRS, CREGU, GeoRessources, 54000, Nancy

*Correspondence: michel.cathelineau@univ-lorraine.fr

Other information

Abbrev. Title: Brine migration, rifting and thrusting in the Pyrenees

Keywords: Triassic evaporite, brine, Pyrenees, mantle exhumation, alpine thrusts, fluid inclusions, fluid mixing.

Salt has often been considered a passive mechanical agent of deformation, favouring nappe displacement thanks to its ductility. Thus, the fundamental characteristic of the salt-forming material is its plasticity, i.e. its ability to flow at low temperatures due to its negligible elastic limit. This creep in the solid-state is linked to the low equivalent viscosity of salt-bearing rocks. In the Pyrenees case, Triassic formations, including clays and evaporitic levels, covered most of the peneplaned Paleozoic basement. A series of works in the ‘70 to ’90s highlighted the role of salt in the pre-alpine deformation, the salt tectonics linked to diapirism (Brinkmann and Logters, 1968; Canérot, 1988; James and Canérot, 1999). Extensional tectonics due to rifting at the end of Cretaceous (Jammes et al., 2009; Tugend et al. 2014; Masini et al., 2014; Teixell et al. 2016; Lagabrielle et al., 2019a and b; Lagabrielle et al. 2020; Labaume and Teixell, 2020) deformed the Mesozoic cover before convergence as fold and thrust belt during Cenozoic. Thus, the last decade emphasised the global geodynamic models of the extension, particularly the rise of the mantle, followed by the Cenozoic compression due to plate movements, and contributed first to putting salt tectonics in the background. Recent works tend, however, to reconsider the role of salt as significant in the local deformation mechanisms at the interfaces between basement rocks and the pile of sedimentary formations in the Mesozoic basins and to propose mixed models (Duretz et al., 2020; Ford and Verges, 2020) as already suggested by Jammes et al. (2009). Pre-rift salt controls the Cretaceous smooth-slopes extensional basins and the subsequent continental rifting mode (Lagabrielle et al. 2020).

Although the geodynamic of the Pyrenees was the subject of considerable progress in recent years, there is still one relatively unexplored dimension: the role of interactions between fluids and evaporites in the dynamics of deformation (formation of breccias, fluid-assisted deformation) and the mass and heat transfers. Interactions between evaporites and percolating waters can contribute to transferring certain chemical elements (Na, K, Ca, Mg), and brine-rock interaction could significantly modify the mineralogy of the percolated rock. Dissolution and cementing processes subsequently produce significant changes in the permeability of drains, particularly along fluid pathways. All the above-cited processes can have significant consequences in fluid dynamics (clogging vs dissolution). The detachments are most often located along with the Triassic formations at the interfaces between basins and Hercynian basement. The very particular location of the Triassic series in the vicinity of the décollement zones, whose initial cause is purely sedimentological and issued from the

paleogeographic history, becomes then the main factor controlling the deformation style, the nature of the migrating fluids and the overall temperature distribution.

Most numerical models of temperature distribution at the crustal-scale do not consider the convection and the role of fluids and admit this shortcoming. However, thermal differences between percolating waters and their host formations can either contribute to heat shallower crustal levels or cool deeper levels along main fluid pathways. Modelling works recognise that this aspect could be essential to consider, but it has not been taken into account so far. However, convection may have occurred in the developing basins and significantly altered the overall thermal regime (Souche et al. 2014). The integration of accurate data obtained on strain-related fluid flow into large-scale geodynamic models would greatly help understand the causes of abnormal heat fluxes and local water-rock interactions along faults.

As there is often a large gap between crustal-scale models and very detailed data that are geographically limited to small perimeters, the objective of this study is to compile large-scale data on paleofluids. In this work, a series of fluid salinity on paleofluids were thus obtained for newly formed minerals crystallised in fractures from the Axial Zone (Paleozoic basement) and its Mesozoic cover all along the Pyrenees. These new data obtained on 14 localities were then compared to the available data from the literature (16 papers providing data from 29 localities), which are somewhat scattered and heterogeneous, and frequently obtained for other purposes than the description of the fluid geochemistry at the belt scale during the main geodynamic events. The present study tries to define the ranges of chlorinity, the degree of mixing and the style of fluid migration during the two main deformation events which have affected the Pyrenees.

Geological context

At the scale of Western Europe, evaporites are widely distributed from Silesia to the Paris Basin, from Aquitaine basin / Biscaye Bay to the south of Iberia (Iberian basin) (Orti et al., 2017). Vast salt basins are also found in North Africa (Leleu et al. 2016; Turner and Sherif, 2007; Courel et al., 2003). The Upper Triassic deposits cover the most significant part of the future Pyrenean area (Fig. 1) and have a thickness ranging from 1000 to 2700 m in the Pyrenees and the Aquitaine Basin (Biteau et al. 2006; Orti et al. 2017). Labaume et Teixell (2020) estimate a thickness of 3000 m for the Middle and Upper Triassic using balancing

constraints for restoration. There are few other equivalent occurrences of such extreme seawater evaporation over hundreds of kilometres after Trias and extension of evaporites, except Messinian salt deposits and some other Cenozoic basins (Babel and Schreiber, 2014). Thus, thousands of kilometres characterise Keuper salt layers. Triassic formations are deposited onto a peneplaned surface almost flat with some islands after a general erosion, weathering and reddening of the outcropping Variscan terranes. The extension of merged areas at that period has mainly been overestimated in the past. Recent works agree on the extension of Triassic layers and the extension of Mesozoic sediments (Liassic formations and Dogger), particularly in zones now free of Mesozoic sedimentary cover as the French Massif Central or the central part of Pyrenees. Evaporites are intercalated between marls and other siliciclastic sediments. Their thickness is generally significant and may vary between a few meters up to hundreds of meters (Orti et al. 2017) and reach more than 1000 m in the Aquitaine basin (Biteau et al. 2006).

The Triassic formations are overlain by a Mesozoic cover whose thickness can reach 3000 m to 4000 m (Teixell et al. 2018; Jammes et al. 2009). The sedimentary cover includes Liassic to Upper Jurassic carbonate platform sediments (Canerot et al., 1978). The syn-rift sediment thickness is locally 5000 m, especially along the Biscaye Bay axis, producing potentially a lithostatic pressure type onto sediments located at the base of the pile, around the transitional depth between hydro- and lithostatic pressures. Evaporites at depth were submitted along the Biscaye rift to more than 6-7 km overlying sediments during the Late Cretaceous, yielding pressures of more than 180 MPa (Duretz et al., 2020).

The role of pre-rift salt in Pyrenean deformation was first described in Jammes et al. (2009). Diapirism is controlled by a crustal-scale extension (Nalpas and Brun, 1993) and is initiated by the overburden faults (Vendeville et al., 1995). Based on analogic modelling, Vendeville et al. (1995) consider that thick salt layers cannot transmit the significant differential stresses necessary for basement faults to propagate upward as faults into the overburden. During extreme crustal thinning and mantle exhumation, the pre-rift sediments were mechanically decoupled from the basement either thanks to the Keuper clays or by the salt layers (Canérot et al. 2001, Clerc and Lagabrielle 2014). The presence of such a kind of décollement layer favoured efficient basement-cover decoupling. Once units are decoupled, deformation can develop independently in the cover and the basement with distinct styles,

both units being separated by significant distances from their initial position. Large salt diapirs may develop when the décollement thickness increases (Duretz et al., 2020).

The early stage of Pyrenean convergence occurred in the Late Cretaceous, with the thrusting of Cretaceous sediments as a pop-up along with the Lakora thrust and North Pyrenean Frontal Thrust (NPFT) (see Fig. 2) in the western Pyrenees (Teixell et al., 2016). A similar deformation style is proposed in the east-central Pyrenees at that time (Mouthereau et al., 2014). Following Teixell (1996), the earliest record of convergence in the vicinity of the two main active thrusts is recorded by the flexural drowning of the Upper Cretaceous shelf limestones in the present-day Axial Zone. The initiation age of "protocollision" is not well defined and could be around 70–75 Ma (Campanian, Mouthereau et al., 2014). During the ''protocollision'', the continental crust recovered its pre-rift thickness. Thrusting was accommodated in the basin by a continued slip of the NPFT and the Lakora–Larra thrust, which experienced a significant displacement at that time and is considered a detachment structure.

During thrusting, basement rocks close to the unconformity with Trias and Cretaceous units were affected by brittle-ductile deformation. In most cases, earlier shear zones (Hercynian or Jurassic) are reactivated, and new tension gashes are formed (Vissers et al., 2020, for instance, at Cap de Creus). In a series of cases, conjugate fault systems and related secondary open structures are associated with the NNE to ENE shortening direction (at Bielsa, Casas et al., 2003) and tight folds accompanied by subvertical schistosity. The low angle dipping quartz-chlorite-calcite veins attest to the subhorizontal shortening (at Bielsa, Bellahsen et al., 2019). Most available data on thrusts indicate a resetting of Ar-Ar ages of Hercynian micas around 50 Ma, particularly along shear zones indicating a high temperature during the alpine deformation peak. Vacherat et al. (2014) and Bosch et al. (2016) infer the maintenance of high temperatures in the North-Pyrenean Zone before the onset of cooling considered to start after 50 Ma. Thus, the fission-track (FFT) studies indicate that cooling starts after 50 Ma and is enhanced mainly after 35 Ma.

Materials

New sampling and data

A series of representative samples were selected from localities covering all Pyrenees from West to East (Fig. 2). Among these samples, two major types of samples were studied: i)

those corresponding to zones of significant water-rock interactions related to syn-rift deformation, ii) those typical of Alpine-style open fractures. The first type is characterised by the development of Mg phyllosilicates (chlorite, talc) in micaschists, dolomitisation in syn-rift carbonate formations and silicification in siliciclastic units (sandstones and quartzites). Several studies consider these water-rock interactions as representative of syn-rift processes and are dated in some instances (albitisation: Poujol et al., 2010, Boulvais et al., 2007; Mg-metasomatism: Boulvais et al., 2006; Boutin et al., 2016; breccias with silicifications and carbonate cements: Debroas et al., (2010), Asti et al., (2019), Incerpi et al., 2020, Nteme Mukonzo et al., 2021, Motte et al., 2021; see later the compilation of available ages). Table 1 provides details about localities (host-rock, inferred ages of the formation when available). Figure 3 and 4 show macro-photographs of silicified and dolomitised breccias (Fig. 3A and B) as well as newly formed assemblages in fractures: euhedral quartz and calcite from Col de Jau (Fig. 3C) and quartz crystals, synchronous of talc, formed in cavities from dolostone at Trimouns (Fig. 3D).

Sets of open fractures are found in the Paleozoic basement rocks from the axial zone, mostly Devonian marbles or siliciclastic facies, close to shear zones. Open veins are either subhorizontal and compatible with the subhorizontal shortening and therefore considered as alpine-style fissures or correspond to reactivated shear planes. At the kilometre scale, thrusts may be inferred but are now eroded, and the Triassic series are only visible close to the NPF in Ariège and Haute Garonne(Fig. 4A and B). Open cavities filled by euhedral quartz may also develop along former faults or shear zones of varied geometries and in newly formed conjugate fault systems. Euhedral quartz (Fig. 4 C and D) are accompanied by simple mineral assemblages (chlorite-calcite). Chlorite is observed in some instances when Fe-Mg minerals are present in the host rocks, such in granites (Lac d'Estaing area), and some euhedral calcite crystals may develop locally on the quartz prisms.

Literature data: available data on salinity and homogenisation temperature were taken from the literature to complete the new data set. In the compilation (Table 2), data were made homogeneous in terms of units. Microthermometric data were converted into salinities when no provided, and all expressed in wt.% eq. NaCl. The distribution of localities is given in Fig. 2.

Most of the literature data on fluid inclusions considered as synchronous of syn-rift or convergence events based on available geochronological data or geological arguments have

been compiled. For a small number of localities, the relation between the available data and the two main events above described is less clear, as the fluid inclusions were studied in older but recrystallised material. Thus, in the case of “old” fault infillings by fluorite, galena or sphalerite deposits, authors consider the earlier mineral assemblages as either Paleozoic or early Mesozoic in age. Such minerals were then deformed and recrystallised later on at unknown periods generally assumed to be Mesozoic (Munoz et al., 2015, Cugerone, 2019). Fanlo et al. (1998) interpret the recrystallisation of fluorite at Parzan as related to the “alpine orogeny” with the expulsion of fluids from sediments during early extensional tectonics, e.g. during rifting, but also consider such fluids as similar to those from the Gavarnie thrust. The similarities between fluid salinity and homogenisation temperatures (Th) of FIs found in these minerals and those related to the rifting/ mantle exhumation stage yield to develop the analogy while remaining cautious on this hypothesis.

Methods

In newly studied samples, fluid inclusion assemblages were observed and defined thanks to optical microscopy with an OLYMPUS BX51 (transmitted and reflected light) optical microscope and a VHX-200 KEYENCE numeric microscope.

Microthermometry was carried out on fluid inclusions (FI) trapped in quartz overgrowths, quartz cement and druzy quartz in sandstone from the sedimentary cover and quartzite from the basement. It was performed using a Linkam® MDS600 heating-cooling stage, adapted to an Olympus® microscope at the GeoRessources laboratory (Nancy, France). The stage was calibrated with in-house and certified standards by measuring the temperature of the final melting of pure water (0.0 °C) in a silica glass capillary, the triple point of CO_2 in a synthetic FI (−56.6 °C), and the homogenisation temperature (L+V→L) of a natural FI at 165°C. The following microthermometric parameters were measured: eutectic temperature (Te), melting temperatures of ice (Tm ice), halite dissolution (Tm NaCl), and homogenisation temperature (L+V→L or L+V+S→L+S; Th). Hydrohalite melting (Tm hh) was not frequently observed. The temperatures of phase changes have a precision of about ± 5 °C for Te, ±0.1 °C for Tm ice, and ±1 °C for Tm NaCl and Th.

Salinity calculations have been made in the H_2O-NaCl system using data from Bodnar and Vityk (1994) based on Tm ice or Tm halite for fluid inclusions containing halite cube (when

Tmh < Th and no Tm hh is available). When both Tm ice and Tm hh or Tm NaCl values were available, salinity was calculated using Steele-MacInnis et al. (2011).

The presence of gas components (CO_2, CH_4, N_2) in the fluid inclusions was determined by Raman spectrometry analysis using a DILOR LABRAM Raman spectrometer at the GeoRessources laboratory, University of Lorraine, Nancy, France.

Results

New data on Fluid Inclusions

Syn-rift occurrences

Salinity and minimal trapping temperatures (Th) are given in Table 1. In syn-rift metasomatic rocks (Reynès, Col de Jau, Trimouns (new data)), both aqueous FI noted Lw and aqueous FI saturated at room temperature with respect to halite noted Lwh are observed. Salinities range from 27 to 35 wt. % eq. NaCl, with modes from 29 to 30 wt. % eq. NaCl, and Th range from 150 to 247°C, with modes from 160 to 220°C. Traces of gas in FI are found in the different localities, mostly N_2-CO_2 with minor CH_4 (Reynès), CH_4 and N_2 (Jau) and both N_2, CO_2 and CH_4 are present in Trimouns FIs with various gas ratios. These new data confirm the presence of high salinity fluids in Mg-metasomatic zones such as those found at Trimouns (Parseval, 1992, Boiron et al., 2007, Quesnel et al., 2019). Such brines appear as predominant in fault zones in the eastern part of the Pyrenees.

Syn-convergence occurrences

Fluid inclusions in euhedral quartz from syn-convergence tension gashes in the Paleozoic basement rock are two-phase FI with size ranging from 5 to 30 µm, and exceptionally 50 to 100 µm (Fig. 5). They are aqueous liquid inclusions (Lw FI), with a vapour phase of about 10-20% and sometimes 25%. FIs in quartz occur either as pseudo-secondary planes, isolated or in small clusters (Fig. 5A, C, E, G) and show in several localities a halite crystal (Lwh FI) (Fig. 5B, D, E and F). The relative amount of Lwh inclusions compared to Lw is less than in the syn-rift metasomatic rocks and silicified breccias. Salinities range from 1.2 to 25 wt. % eq. NaCl, with modes from 1.7 to 25 wt. % eq. NaCl. More in detail, at La Calabasse, Coulédous or Val d'Alet, salinities are high, above 20 wt. % eq. NaCl and are limited to a narrow range. At Alzen, Balacet, Vallée d'Aspe (La Cristallère or Portalet), the ranges are also small but values are around 8-10 wt. % eq. NaCl, and 15 wt. % eq. NaCl at St Lary and Estaing. The lowest values (mode at 1.7 wt. % eq. NaCl), lower than seawater salinity, were only recorded at Val

d'Aran. Th range from 108 to 235°C, with modes from 110 to 200°C, and up to 230°C at Estaing and Saint Lary. Traces of gas are found, mostly CO_2 with minor CH_4 and N_2 (La Calabasse, St Lary) and a predominance of N_2 in other localities (Val d'Aran, and Val d'Alet, for instance).

Literature data

The main features of FIs described in the literature data are compiled in Table 2.

Syn-rift processes

In Chainons Bearnais (Salardon et al., 2016, Corre et al., 2018, Nteme Mukonzo et al., 2021, Motte et al., 2021), salinities of FI in cements synchronous of the rift climax, range from 10 to 37 wt. % eq. NaCl, with modes from 14 to 34 wt. % eq. NaCl. Most of the salinity modes are higher than 20 wt. % eq. NaCl. in 90% of the localities. It can be noted that lower salinity fluids (up to 7.5 wt. % eq. NaCl) are observed in dolomites (DC2 to DC3 in Mano formation, Motte et al., 2021) related to early diagenesis. Syn-rift fluids have Th ranges from 130 to 280°C, with a few data between 300 and 340°C (dolomite rim, Salardon et al., 2016, syn-rift Dolomite DC4 - Mano, Motte et al., 2021). Th are lower in areas where the sedimentary cover was thinner such as Rousse and Deep Lacq (dolomite in the Mano dolostone at Rousse (Renard et al., 2019) and Deeper Lacq (Bahnan, 2019)). Traces of gas such as CO_2, CH_4, N_2 and H_2S were found in most localities in Chainons Bearnais, with variable relative amounts depending on the location.

In the Mesozoic cover, north to NPFT, salinities are much lower (mode at 3.5 wt. % eq. NaCl at Rousse (Renard et al., 2019). In Deep Lacq, higher salinities ranging from 8 to 10 eq. wt. % NaCl are due to Triassic fluid inputs (Bahnan, 2019).

Syn-convergence processes

In the thrust fault areas, particularly the Gavarnie-Neouvielle area (Banks et al., 1991, McCaig et al., 2000), salinities range from 5 to 34 wt. % eq. NaCl, covering an extensive range of values between these extrema, and Th range from 110 to 230°C. In Monte Perdido (Lacroix et al., 2011), salinities are very low, around 1.6 wt. % eq. NaCl, probably due to the isolation of Ypresian formation from Triassic brines.

In the Mesozoic cover, north to NPFT: in Upper Lacq, dolomite and calcite formed from relatively dilute fluids (Bahnan et al., 2020) probably due to the isolation of the upper

reservoir and to the proximity from the surface. Alternately Bahnan (2019) describes in the deep Lacq reservoir higher salinity fluids (9-14 wt. % eq. NaCl) during the early convergence stage, as Renard et al. (2019) in syn-convergence fault breccia from Rousse.

Reworked ore deposits

Fluid inclusion data from ante-Triassic ore deposits (fluorite and Pb-Zn) in the Central Pyrenees were considered because they are deemed to be affected by later undefined age events sometimes inferred as "Mesozoic" s.l. (Subias and Fernandez-Nieto, 1995; Johnson et al., 1996; Munoz et al. 2015; Cugerone, 2019). In these localities, most salinities are above 10 wt. % eq. NaCl, and up to 39 wt. % eq. NaCl. Early quartz at Cierco (Johnson et al., 1996) contains high salinity FIs (28 % eq. NaCl). At Argut and Pal de Rase (Cugerone, 2019) or Portalet (Subias and Fernandez – Nieto, 1995), salinities are lower and range from 1 to 10 wt. % eq. NaCl. A 150-280°C Th range was found in most studies at the exception of the Lacore and Argentieres deposits where Th are lower (110-140°C at Les Argentières, up to 180°C at Lacore: Munoz et al., 2015).

General trends

The distribution of all the available data indicates a complete range of salinities between high salinity of Lwh FI, which are saturated with halite at room temperature and low salinity fluids (Fig. 6). In a given sample and locality, the salinity displays in general a narrow range. Th ranges are in some instances indicative of a variety of densities, in particular in the case of Cretaceous occurrences. Such ranges may be attributable to pressure fluctuation, as stretching is limited in quartz and stretched FI carefully discarded.

Discussion

Mixing between brines and low salinity fluids

Two distinct trends are observed in the Th-salinity diagrams (Fig. 6): i) a trend between an end-member of low salinity close to seawater chlorinity, with Th around 250°C, and an end-member with high salinity, slightly cooler (syn-rift process) (Fig. 6A), ii) a trend between a similar saline end-member than that of the first trend, and a dilute end-member even less saline than seawater, with significantly lower Th than the brine (Fig. 6B). These two trends

tend to discriminate a series of localities considered representative of fluid migration during the two distinct main geodynamic stages.

The first trend corresponds to the Cretaceous extension with Na (Mg, Ca or Si) metasomatism in basement formation either from the eastern part of the Pyrenees (Reynès, Jau, Trimouns) or western occurrences (Urdach, for instance). Most samples come from locations close to the boundary between the Paleozoic basement and the Mesozoic sedimentary formations, e.g. close to highly deformed remnants of the pre-rift cover, including Triassic units.

The second trend (Fig. 6 B) is typically representative of the thrusts, especially the Gavarnie thrust, where Triassic units are pinched in between syn-rift sediments, both being thrusted onto the basement. The lower Th of the recharge fluids and the potential low salinity of the end-member could indicate that meteoric fluids are entering the system from above and mix along subvertical or high angle faults, such as proposed for the Néouvielle massif by McCaig et al. (2000).

Fig. 6C provides salinity-Th envelopes for reworked ore deposits. High salinities were found in Zn-deposits considered affected by Mesozoic events (Lacore and Les Argentières, Munoz et al., 2015, Crabioules and Victoria, Cugerone, 2019). A series of other localities display similarities with the values found in syn-convergence occurrences (Cierco, Johnson et al., 1996; Tebarray, Lanuza and Portalet, Subias and Frenandez-Nieto, 1995).

Figure 7 presents the distribution of salinity per locality in a box plot with range and mode values for the three main categories: reworked ore deposits, syn-rift and syn-convergence (both thrusts and open fractures). The salinity ranges recorded locally in a locality are of two types: i) a salinity whose values are narrowed around a mean value indicating a mixing process elsewhere but not in the trapping zone. Therefore, the mixing product is exported from its production zone and then trapped as a fluid with a homogeneous salinity and, ii) populations of FIs with a wide salinity range indicative of in situ mixing between the two end-members (Fig. 7).In both cases, the saline end-member has all the features of evaporitic brines, equilibrated in temperature with their host formations, particularly chlorinities up to 30-35% close to halite saturation at 250-300°C (Fig. 7).

At Trimouns, several data agree with the features of the primary evaporitic brines, such as the richness in Na-K-(Mg), Cl isotopes values compatible with evaporated seawater, and a low Cl/Br ratio indicative of evaporated seawater having passed halite saturation, at less for

a part of the data (Quesnel et al., 2019). The calcium content is relatively high as in most other similar brines and is generally interpreted as Na-Ca exchange result through brine-rock interactions such as albitisation (McCaig et al., 2000, Boiron et al., 2010). Primary and secondary brines probably mixed as shown by the complete range of Cl/ Br (molar ratio) from 200 above 1000 in syn-rift fluids (Trimouns, Quesnel et al., 2019) and in syn-thrust fluids, 100-250 (at Pic Long and La Glère (Neouvielle Massif) to 1000 - 3000 (at Gistaing and Plan de Larri, close to the Triassic red beds at the unconformity with the basement (McCaig et al., 2000)). At Col d'Etche, close to the Urdach lherzolite, syn-rift fluids are only secondary brines with Cl/ Br ranging from 2000 to 2320 (Nteme Mukenzo et al., 2021).

For the late Cretaceous events linked to rifting, the most probable end-member is seawater as the region was covered mainly by Albian to Cenomanian sea. For the Cenozoic events, brines are diluted by a low salinity end-member with a lower temperature, the mixing producing intermediate salinities down to that of seawater. At Gavarnie, the recharge fluids are interpreted as meteoric waters as the relief permitted to imply such water input as shown by isotopic data (McCaig et al., 2000; Trincal et al., 2017). In sedimentary reservoirs close to the North Pyrenean Frontal Thrust (NFPT) such as Rousse and Deep Lacq, post-rift fluids are still influenced by inputs (Cl, sulfate) from Triassic formations (Renard et al., 2019, Bahnan, 2019).

Predominance of brines at the belt scale

The map from Fig. 8 shows that from west to east, saline fluids are omnipresent at the scale of Pyrenees, all along the axial zone whatever the considered event. There is no specific distribution as brines as the highest salinities are encountered in all parts of the chain. However, localities with the lowest salinities are more frequent north of the North Frontal Pyrenean Thrust (NFPT) in the Cretaceous sedimentary cover, north of the axial zone, and along some thrust zones such as Plan de Lari or Gistain (McCaig et al., 2000). Even low (5-10 wt.% eq. NaCl), salinities remain above the seawater salinity for most localities, except at Monte Perdido, where salinity mode is around 1.6 wt.% eq. NaCl (Lacroix et al., 2011).

The chlorinity ranges, which indicate mixing between contrasted salinities fluids, are more or less pronounced depending on localities. The most extensive range is reported at Gistain and Parzan (thrusts, McCaig et al. 2000; Fanlo et al. 1998), but also in the Chainons Bearnais at Urdach and Saraille, where processes are attributed to the rifting stage (Salardon et al.,

2016, Corre et al. 2018; Nteme Mukonzo et al. 2021). Thus, mixing processes occurred during the two main deformation events.

Although most fluids are much above seawater salinities, both Figures 7 and 8 show that the range of salinities cover significantly lower values in material from thrusting zones (in blue in Fig. 7) than in Cretaceous metasomatic zones where most of FI populations include brines with maximal salinities (in red, in Fig. 7). Exceptions are the high salinities found in thrust zones at La Glere and Pic Long and Pic de Port Vieux in zones close to Triassic sediments. Thus, brines flew along thrusting zones, probably escaping from sheared or squeezed Triassic formations, like those found along with the Gavarnie thrust (McCaig et al., 2000). A brine end-member is thus present during the major stages of Alpine thrusting.

In syn-convergence fissures from the Paleozoic basement in the Axial zone, FI salinity ranges cover a few weight % eq. NaCl in a given locality, but the data envelopes for all alpine fissures define an alignment superimposed on the series of data already described along main thrust zones such as Gavarnie by McCaig et al. (2000). The whole data set constitutes a nearly continuous trend indicative of varied mixing rates between low and high salinity waters. As the mixing does not occur in fluid trapping, the mixing rate is typical of each locality. As a preliminary conclusion, most alpine fissures formed from saline fluids corresponding to different mixing rates between the saline and dilute end-members. Thus, the Paleozoic basement was penetrated by brines at all scales in the vicinity of significant faults. As fluids display the same features in small fissures or damaged zones as along significant faults and thrusts, migration of brines and dilute fluids can be considered as driven by major pathways, together with a fissure permeability at all scales (tension gashes, joints and faults).

The chlorine reservoir

During Upper Triassic, the deposition of clay and salt layers is at the origin of a considerable mass of chlorine as halite covering more than 40000 km^2 (an approximatively minimal surface for the present-day Pyrenean belt: 400 km long by 100 km large). The shortening has reduced by around 30% the pristine surface of the evaporite. The mean thickness is difficult to estimate: salt layers vary from tens of meters up to 360 m thickness for the Anisian layers (Orti et al., 2017) or even more than 1000 m in the Aquitaine basin. Taking a minimal estimate of 50 m, the pristine surface of evaporites, a minimal estimation of a salt volume

of 2600 km^3, thus a part of the 50 000 km^3 of west European Keuper salt (Evans, 2006, Ryan, 2008). The specific location of evaporites at the boundary between the Paleozoic basement and the Mesozoic cover has favoured major detachments. In this process, evaporite layers were squeezed, yielding to the subsequent release of primary brines. Water is present in rock salt as interstitial water and as fluid inclusions (Dubessy et al., 1983, Urai et al., 1986). The amount of primary brines as fluid inclusions or pore fluids within the halite are estimated to reach up 1 to 5 % in volume, as shown by microphotographs in Dubessy et al. (1983). Taking minimal estimates of 1 to 2% of brines in salt layers, the primary brine volume could reach a minimal volume of 26 to 52 km^3. Besides, brines in salt play a significant role in the creep of rock salt by pressure-solution (Spiers et al., 1990) and can move in salt under thermal gradients (Shao et al., 2019). Secondary brines issued from halite dissolution can also increase the total brine volume.

Triassic chlorine salt source versus serpentinisation salt

The results of this compilation indicate that Triassic evaporites constitute a significant source of chlorine that may have been moved at several periods since Triassic times: first, close to sedimentation periods are at the origin of the local formation of red beds concentrations (Subias et al., 2015); second, during Mesozoic at unknown ages, remobilisation of early metal stock as proposed by Munoz et al.(2015) and Cugerone (2019); third, during the Cretaceous rifting, major convective fluid movements occurred under enhanced thermal gradients produced by the mantle exhumation (Quesnel et al., 2019); fourth, during Cenozoic, fluid displaced along with major thrusts during convergence (McCaig et al., 2000), in particular along sliding zones such as clay and evaporite formations, and their vicinity such as damaged zones. Chlorine is still present at varying concentrations in all thermal waters exploited all along the chain, in localities the most frequently very close to Triassic units pinched along major faults and thrusts. The best examples are located along the NFPT: Salies du Salat near Betchat and Salies du Bearn. Saline thermal waters are also recognised in the area of Eaux Chaudes thrust and close to the NPF around Bagnères de Bigorre (Levet et al., 2002), indicating that remaining chlorine can be still mobilised.

For the particular Cretaceous mantle exhumation stage, new concepts have put forward brine formation by interactions between mantle rock and seawater. Hovland et al. (2018) reviewed the different hydrothermal processes which should produce salt and brines

through hydrated mineral formation, a mechanism already proposed by several studies (Gleeson et al., 2003, Stober and Bucher, 2004, Richard et al., 2013, Bons et al., 2014, Walter et al., 2016, Martz et al., 2019). Scribano et al. (2017) have suggested that the formation of giant salt deposits should be genetically related to the serpentinisation of ultramafic rocks. Thermodynamic calculation confirms the feasibility of salt formation through the consumption of massive amounts of seawater by serpentine crystallisation at the expense of olivine and a mechanism of salt precipitation by decreasing the hydrothermal solution temperature down to 4°C on the seafloor (Debure et al., 2019). However, this salt formation model does not apply to our deep (more than 3-5 km) systems, where the temperature was maintained around 200-300°C. The brine genesis is feasible in serpentinised mantle rocks and depends on water-rock ratio, temperature, and pCO_2. Alternately, the masses of Triassic and Infra-Lias salt reservoir constitute a huge Cl reservoir able to produce by squeezing significant amounts of potential primary, or though dissolution, secondary brines at the same time as serpentinisation.

In the case of Pyrenees, the processes of serpentinisation can mostly be invoked for the rifting stage. Thus, the source of Mg responsible for Mg-metasomatism in silicate rocks and dolomitisation in limestones was frequently attributed to a release of Mg during the serpentinisation process. First of all, serpentinisation is not supposed to release significant amounts of Mg as reactions may be written with conservative Mg. Primary evaporitic brines are also particularly enriched in Mg, which concentration increases continuously with the evaporation rate, the bischofite ($MgCl_2$-$6H_2O$) saturation being never reached (Fontes and Matray, 1993). Even in the case of the syn-rift formation of Trimouns Mg-metasomatic halos around 115-100 Ma (Schärer et al., 1999; Boutin et al., 2016), Quesnel et al. (2019) precluded serpentinisation as the main source of chlorine of brines at the origin of talc formation. Thus, most geochemical parameters of brine fluid inclusions, although not incompatible with other processes such as dehydration processes, are close to Triassic evaporated seawater. The low Cl/Br ratios, for instance, below those of seawater, are not explained easily by simple water uptake and necessitate specific Br enrichment processes, such as evaporation after halite saturation. Cl/ Br ratio lower than that of seawater (90 to 400), thus after evaporation, were found at Trimouns, but also in the Gavarnie thrust (Banks et al., 1991, McCaig et al., 1995, 2000, Table 2) and other rifts such the Iberian rift from Asturias to the Maestrat basin (Grandia et al., 2003 a and b, Sanchez et al., 2009). Applying

Occam's Razor rule, the localisation and abundance of salt along detachment zones where fluids have migrated is such that it is by far the most likely to search the chlorine source there rather than in any other remoted area or process.

P-T conditions of trapping

P-T reconstructions necessitate independent geothermometry as the aqueous fluid inclusions are only characterised by their density and salinity. Trapping occurred at any P-T pair along with FIs representative isochores. Either independent temperature estimates are needed, or hypotheses are required for the geothermal gradients. Two main independent estimates are found in the literature: chlorite geothermometry for some localities and a more comprehensive data set is now available on the organic matter at the scale of the Pyrenees using Raman geothermometry on organic matter (Clerc et al., 2015, Saspiturry et al., 2020) and more detailed zones such as the Chainons Bearnais (Izquierdo-Llaval et al., 2020). The brines related to rift conditions were trapped at Trimouns around 300- 350°C using chlorite thermometry, thermal gradients, and fluid inclusion data (Boiron et al., 2007, Boutin et al., 2016, Quesnel et al., 2019). In Chainons Béarnais, estimates are around 240-280°C at Urdach (FI data, Nteme Mukonzo et al., 2021) and 190-280°C at Sarraillé (FI and chlorite data, Corre et al., 2018). For the thrusts, several indications are provided by chlorite geothermometry (Trincal et al., 2015, 2017) with temperatures around 300 to 350°C, and in exceptional cases above 400°C). Thus, the two main periods of fluid migration occurred within the same temperature range (300± 60°C).

Periods of brine migration in the Pyrenees

Brines are present since the deposition of evaporitic levels. Some authors do not exclude that these brines were responsible during Upper Trias or slightly later for metal transport and deposition in permeable horizons such as sandstones (Subias et al., 2015). Main periods of brine migrations and fluid mixing in the Pyrenees are, however, later, as shown in Figure 9, which presents a summary of available ages (water-rock interactions (Na, Ca-Mg metasomatism, deformation (mylonitisation, magmatism, thrusting) for the two considered periods: the Cretaceous mantle exhumation and rifting, and the period of convergence with the pop-up structure of the axial zone. Before mantle exhumation, the temperature close to the boundary between the Palaeozoic basement and the sedimentary cover was a function

of the thickness of the deposited post-rift sediments before rifting. There is little evidence of significant brine migration up to the mid-Cretaceous. Exceptions could be localised fluid flows along discontinuities as those described around the 150 Ma event (Cathelineau et al., 2012, Boiron et al., 2010) to the north of the Aquitaine basin, and which have also been described or invoked in the Pyrenees (Boutin et al., 2016, for the chlorite stage dated around 160 Ma at Trimounss, Munoz et al., 2015, Cugerone, 2019 for the Pb-Zn occurrence), and Spain (Sanchez et al., 2010). The link between these events, such as those dated at Trimouns (Boutin et al., 2016) and the implication of brines, is not entirely proven.

It is difficult to estimate the relative impact of the two deformation stages in reworked ore deposits and when fluids were trapped exactly. However, the salinity-Th pairs of the trapped fluids indicate remarkable similarities with fluids described elsewhere in the present work (Fig. 6). Thus, some fluids have features similar to those of syn-rift occurrences, and others display a better match with syn-convergence localities, as shown in blue in Fig. 6C. Absolute dating would be necessary to ensure these correlations to geodynamic events.

Role of salt and brines during the rifting stage

Ages for the rift period and main metasomatism stages range from 120 to 98 Ma (Fig. 9). Both deformation and temperature promoted salt flowing, e. g. diapirism, and reversely the presence of enhanced displacements due to salt plasticity. Salt has an effective viscosity vary from 10^{17} to 10^{20} Pa.s below the equivalent viscosity of other rocks (Carter and Hansen, 1983, van Keken et al., 1993) and a density around 2,1 g/cm^3 (Urai et al., 2008) generally below the density of other sediments which are compacted, dehydrated and cemented during diagenesis and burial. When the temperature rises, the salt viscosity decreases according to an exponential law and therefore increases its plasticity. Pressure reduces the salt viscosity and favours its mobility, contrary to other surrounding rocks (carbonates, sandstone, clays), for which diagenesis progressively increases the viscosity. Besides, salt contains water which weakens its mechanical properties (Urai et al., 2008) and participates in pressure solution governing creep (Spiers et al., 1990). The peculiar properties of salt explain the halotectonics and the prominent role of salt in the Pyrenean tectonic evolution. It can be noted that the presence of water lowers the viscosity of the salt and allows it to behave like a quasi-Newtonian fluid. Therefore, brines present at the grain boundaries within the evaporites enhance the deformation of the evaporite formations.

555 Temperature affects the rheology of saline rocks by lowering the viscosity of salt. In the
556 Pyrenees, the significant increase of temperature due to mantle uplift yields to halite
557 flowing. Thus, heat and temperature gradients substantially affect a thick layer of salt
558 (Jackson and Talbot, 1986) and favour gravity instability and subsequent diapirism (Fig. 10 A,
559 B). Therefore, it is logical that the first stage of diapirism and salt tectonics occurred during
560 the Cretaceous rifting period of increased thermal gradients. The importance of crustal
561 extension in diapirism initiation was thus recognised in the Pyrenees (Brinkmann and
562 Logters, 1968; Masini et al., 2014; Duretz et al., 2020). Together with the temperature effect,
563 the tectonic regime during pre- and syn-rift stages had also significant consequences on the
564 localisation of salt flows (Canerot et al., 2005). The early history of rifts is mainly put
565 forward, especially the extension of the pre-rift deposits during mid-Cretaceous rifting, or
566 even during Jurassic, with an early salt mobilisation in relation with basement faulting,
567 followed by later gliding of evaporites during the rift climax (Labaume and Teixell, 2020).
568 Brines were trapped at relatively high temperatures between 250°C and 350°C at Trimouns
569 and Urdach, taking trapping temperatures (Th corrected from pressure). Main salinity-Th
570 trends from Fig. 6 underline the similarity of the salinity-Th pairs of the hypersaline fluids
571 and the mixing trend between these brines and a hotter dilute end-member, inferred as
572 seawater. Waters entering in contact with the denudated mantle just above the rift axis
573 during the rifting stage could have undergone overheating. Heated seawater could have
574 brought heat when coming from abnormal temperature areas (Fig. 10B and C). Laterally,
575 strong temperature gradients favoured fluid convection, major fluid pathways being the
576 decollement planes. The venue of these hot waters along the sliding planes of the Triassic
577 units and their mixing with brines may have triggered water-rock interactions and facilitated
578 movements on the planes of detachment. At the end of the rifting process, upper
579 Cretaceous sediments could have acted as fluid barriers and may explain that brines become
580 the predominant fluids again, as seawater do not enter anymore in the system (Fig. 10D and
581 E). Such a process was inferred in the case of the late silicification at Urdach: mixing trends
582 between saline and dilute end-members are typical of the early silicification, and during later
583 stages, quartz cement formed from hypersaline brine suggesting that the unconformity was
584 isolated due to the deposition of the Cenomanian flysh, limiting or stopping the venue of
585 seawater (Nteme Mukonzo et al., 2021).
586

Brines and salt during the convergence stage

The remaining halite bearing formations, when not entirely dislocated during the rifting stage, and the diapiric structures have been rejuvenated and reactivated during shortening. For instance, squeezing and welding of the diapiric zone from the upper European margin formed the NPFT (Labaume and Teixell, 2020). Thus, thrusting benefited from the peculiar rheological properties of Triassic evaporite/clay levels. The beginning of convergence (proto-collision following Vacherat et al., 2014) is proposed around 84 Ma (Labaume and Teixell, 2020), with subduction of a thin crustal domain (Mouthereau et al., 2014). Thrusting is dated around 45-35 Ma in the Gavarnie region (38 Ma for the Eaux Chaudes, 33,5 Ma for Gavarnie thrust (Rahl et al., 2011), younger ages in the Spanish part (33-20 Ma), synthesis in Labaume et al., 2016), and to the east of the Pyrenees around 42-49 Ma along with the Pedraforca thrust (Cruset et al., 2020) (Fig. 9). The period of brine migration during thrusting is, therefore, shorter than during the Cretaceous rifting.

Along thrust faults, fluids interact with Triassic evaporites as suggested by strontium isotopic data (for instance, Cruset et al., 2020 at Pedraforca). Meteoric waters during their downward migration from highs are probably in thermal disequilibrium and consequently cool the fault damaged zone (Fig. 11). The anisothermal mixing between hot brines with shallower and cooler fluids occur when faults and major thrusts bring the two fluid end-members in contact.

Schema from Fig. 11 A emphasises the potential fluid pathways of Triassic brines all along with the thrusts and their mixing with meteoric waters, downward infiltrated from highs. Away from the main thrusting planes, fluids may also mix in brittle structure networks and damaged zones around faults such as in the Néouvielle massif. In such a model, meteoric waters are cooler than brines issued from more profound levels. The mixing is thus anisothermal and explains the generalised trend from Fig. 6B. In the Ariège area (Fig. 11B), below the overlying thrust zones now eroded, fluids infiltrate vertically, thanks to the subvertical structures in the Paleozoic basement, and precipitate quartz in tension gashes close to active shear faults (Fig. 11C).

Convergence is followed by a period of quick exhumation between 35 and 25 Ma, synchronous of the collision cessation (Mouthereau et al., 2014), with subsequent cooling (Fillon et al., 2021) and easier penetration of surface waters. During the post-orogenic

exhumation phase and up the to present day, meteoric inputs are predominant (saline thermal waters).

Conclusions

The main conclusions are as follows:

- During Upper Triassic, the deposition of clay and salt layers is at the origin of a huge mass of chlorine as halite covering more than 40000 km^2. Using a minimal value of 50 m thickness, the estimated salt volume is 2600 km^3. The specific location of evaporites at the boundary between the Paleozoic basement and the Mesozoic cover has undoubtedly played a major role in forming the detachments. In this process, evaporite layers were squeezed, leading to the subsequent release of primary brines. The pristine volume of primary brines as fluid inclusions and interstitial fluids could have reached a few tens of km^3.
- During rifting stages, the very particular location of the Triassic evaporites in the vicinity of the décollement zones yielded Triassic formation played a prominent role in detachment zones where the upper crust basement was in contact with both the exhumed mantle and the pre-rift sedimentary cover. Primary brines were primarily expulsed during extension and then relayed by secondary brines produced by evaporite dissolution by seawater. Their mixing produced a series of fluids with a chlorinity covering a vast range from 35 to 5 wt. % eq. NaCl.
- During convergence, evaporitic layers played a mechanical role, particularly well exposed along the Gavarnie thrust. Meteoric waters were implied in the mixing processes during convergence. Production and migration of fluids occur from Triassic times to the end of Cenozoic, therefore for a much more extended period than that the potential formation of brines by mantle rock-water interactions, such as serpentinisation.
- Consequently, the debate about the respective roles of Triassic brines and mantle-seawater interactions derived brines concerns a relatively short period compared to the rather long period of movements recorded for the Triassic brine migrations. Suppose the dewatering could be the cause of chlorinity increase of fluids entering mantle rocks during the late Cretaceous, it could be, therefore, a further cause of

chlorinity increase. The substantial initial chlorine reservoir remains, however, undoubtedly the most significant contribution to the occurrence of brines circulating during a long-lasting period in the Pyrenees.

- As a whole, the evaporitic Triassic series played a role in all stages of the Pyrenees evolution. The most remarkable feature of fluids in motion by the several geodynamic episodes is their high salinity, a significant part being close to equilibrium with halite. The other part is a product of partial mixing with waters entering from upper levels.
- Although separated by 50-70 Ma, the two deformation events (syn-rift extension and thrusting) are characterised by a similar fluid mixing pattern involving the same salt end member. During both events, the temperature conditions are identical (300± 60°C), raising the question of temperature evolution between the two events and the existence of relatively high gradients over a reasonably long period.
- In the deposits considered ante-Triassic in the Axial zone, fluid inclusions display very similar salinity and density to those described in the syn-rift and syn-convergence fractures. Despite the absence of absolute dates, this analogy suggests that the fluids at the origin of the remobilisations correspond to one of the two main events that affected the Pyrenees.

Acknowledgements

Work on Pyrenean paleofluids has been initiated for many years thanks to the collaboration with colleagues from Geosciences Rennes (P. Boulvais, Y. Lagabrielle) and benefited from recent discussions with Y. Lagabrielle at the occasion of the study of Urdach fluids. New data presented here are issued from a Licence stay of Hugo Jakomulski realised in 2017-2018 at GeoRessources. The data compilation, carried out in late 2020, has been besides stimulated during the simultaneous scientific program “Fluids” by TOTAL and discussions with E. Gaucher and S. Calassou in the preceding years, as well as B. Quesnel during his post-doctoral research at CREGU on Mg-metasomatism. F. Ferracin is thanked for providing excellent material from Ariège quartz-filled fractures and observations. Mar Moragas and David Banks are warmly acknowledged for their constructive and valuable reviews and Giovanni Camanni for editorial handling.

682 **Author contributions**

683 **MC:** conceptualization (lead), interpretation, writing

684 **MCB:** conceptualisation (supporting), data reduction and synthesis

685 **HJ:** petrography and microthermometry on fluid inclusions

686

687

688

689 **References**

690

691 Asti, R., Lagabrielle, Y., Fourcade, S., Corre, B. and Monié, P. 2019. How do continents
692 deform during mantle exhumation? Insights from the northern Iberia inverted paleo-passive
693 margin, western Pyrenees (France). *Tectonics* **38**, 1666–1693. DOI: 10.1029/2018TC005428.

694

695 Babel, M. and Schreiber, B. 2014. Geochemistry of Evaporites and Evolution of Seawater,
696 Treatise on Geochemistry. Elsevier, **9.17**, 483-560. DOI: 10.1016/B978-0-08-095975-7.00718-
697 X

698

699 Bahnan A.E., 2019. Fluid circulation and diagenesis of the Lacq Petroleum System: Impact of
700 the geodynamic evolution. PhD thesis, Univ of Lorraine, 218 p.

701

702 Bahnan, A.E., Carpentier, C., Pironon, J., Ford M., Ducoux, M., Barré, G., Mangenot, X. and
703 Gaucher E.C. 2020. Impact of geodynamics on fluid circulation and diagenesis of carbonate
704 reservoirs in a foreland basin: Example of the Upper Lacq reservoir Aquitaine basin, SW
705 France). *Marine Petroleum. Geology***, 111**, 676-694.

706

707 Banks, D.A., Davies, G.R., Yardley, B.W.D., McCaig, A.M. and Grant, N.T. 1991. The chemistry
708 of brines from an Alpine thrust system in the Central Pyrenees: an application of fluid
709 inclusion analysis to the study of fluid behaviour in orogenesis. *Geochimica Cosmochimca*
710 *Acta*, **55**, 1021-1030

711

712 Bellahsen, N., Bayet, L., Denele, Y., Waldner, M., Airaghi, L., Rosenberg, C., Dubacq, B.,
713 Mouthereau, F., Bernet, M., Pik, R., Lahfid, A. and Vacherat, A. 2019. Shortening of the axial
714 zone, Pyrenees: Shortening sequence, upper crustal mylonites and crustal strength.
715 *Tectonophysics*, **766**, 433-452.

716

717 Biteau, J.J., Le Marrec, A., Le Vot, M. and Masset, J.M. 2006. The Aquitaine Basin. *Petroleum*
718 *Geoscience*, **12**, 247–273. DOI: 10.1144/1354-079305-674.

719

720 Bodnar, R.J. and Vityk, M.O. 1994. Interpretation of microthermometric data for H_2O-NaCl
721 fluid inclusions. In: Fluid Inclusions in Minerals, Methods and Applications, B. De Vivo and M.
722 L. Frezzotti, eds, pub. Virginia Tech, Blacksburg, 117–130.
723
724 Boiron, M.C., Cathelineau, M., Dubessy, J., Fabre, C., Boulvais, P. and Banks, D.A. 2007. Na-
725 Ca-Mg rich brines and talc formation in the giant talc deposit of Trimouns (Pyrenees): fluid
726 inclusion chemistry and stable isotope study. European Current Research on Fluid Inclusions,
727 Bern, p. 90.
728
729 Boiron, M.C., Cathelineau, M. and Richard A. 2010. Fluid flows and metal deposition near
730 basement/cover unconformity: Lessons and analogies from Pb-Zn-F-Ba systems for the
731 understanding of Proterozoic U deposits. *Geofluids*, **10**, 270-292.
732
733 Bons, P., Fusswinkel, T., Gomez-Rivas, E., Markl, G., Wagner, T. and Walter, B. 2014. Fluid
734 mixing from below in unconformity-related hydrothermal ore deposits. *Geology*, **42**, 1035-
735 1038.
736
737 Bosch, G.V., Teixell, A., Jolivet, M., Labaume, P., Stockli, D., Domenech, M., and Monié, P.
738 2016. Record of Eocene-Miocene thrusting in the western Axial Zone and Chaînons Béarnais
739 (west-central Pyrenees) revealed by multi-method thermochronology. *Comptes Rendus.*
740 *Geosciences,* **348**, 246-256.
741
742 Boulvais, P., de Parseval, P., D'Hulst, A. and Paris, P. 2006. Carbonate alteration associated
743 with talc-chlorite mineralisation in the eastern Pyrenees, with emphasis on the St.
744 Barthelemy Massif. *Mineralogy Petrology*, **88**, 499–526.
745
746 Boulvais, P., Ruffet, G., Cornichet, J. and Mermet, M. 2007. Cretaceous albitization and
747 dequartzification of Hercynian peraluminous granite in the Salvezines Massif (French
748 Pyrénées). *Lithos,* **93**, 89–106.
749
750 Boutin, A., de Saint Blanquat, M., Poujol, M., Boulvais, P., de Parseval, P., Rouleau, C., and
751 Robert, J.F. 2016. Succession of Permian and Mesozoic metasomatic events in the Eastern

752 Pyrenees with emphasis on the Trimouns talc-chlorite deposit. *International Journal of Earth*
753 *Sciences,* **105,** 747–770.
754
755 Brinkmann, R. and Logters, H. 1968. Diapirs in Western Pyrenees and Fore-land Spain. In:
756 Diapirism and Diapirs: A symposium (Ed. by BRAUNSTEIN J. and O'Brien. G.). *American*
757 *Association Petroleum Geology*, **8**, 275-292.
758
759 Canals, A., Cardellach, E., Moritz, R. and Soler, A. 1999. The influence of enclosing rock type
760 on barite deposits, eastern Pyrenees, Spain: Fluid inclusion and isotope (Sr, S, O, C) data.
761 *Mineralium Deposita,* **34,** 199-210.
762
763 Canérot, J. 1988. Manifestations de l'halocinèse dans les chaînons béarnais (Zone Nord-
764 Pyrénéenne) au Crétacé inférieur. *Comptes-Rendus Académie Sciences*, **306,** 1099–1102.
765
766 Canérot, J., Peybernes, B. and Cizsak, R. 1978. Présence d'une marge méridionale à
767 l'emplacement des Chaînons Béarnais (Pyrénées basco-béarnaises). *Bulletin Société*
768 *Géologique de France*, **7(20),** 673–676.
769
770 Canérot, J., Majesté-Menjoulas, C. and Ternet, Y. 2001. La faille Nord- Pyrénéenne, mythe ou
771 réalité ? Le couloir de décrochement de Bielle–Accous, élément de réponse du terrain en
772 Aspe et Ossau (Pyrénées-Atlantiques). *Strata*, **2-37**, 1–36.
773
774 Canérot, J., Hudec, M.R. and Rockenbauch, K. 2005. Mesozoic diapirism in the Pyrenean
775 orogen: Salt tectonics on a transform plate boundary, *AAPG Bulletin,* **89**, 211–229,
776 https://doi.org/10.1306/09170404007
777
778 Carter, N.L. and Hansen, F.D. 1983). Creep of rocksalt. *Tectonophysics*, **92**, 275-333.
779
780 Casas, A.M., Oliva, B., Roman-Berdiel,T. and Pueyo E. 2003. Basement deformation: Tertiary
781 folding and fracturing of the Variscan Bielsa granite (Axial Zone, central Pyrenees),
782 *Geodynamica Acta*, **16**, 99–117.
783

784 Cathelineau, M., Boiron, M.C., Fourcade, S., Ruffet, G., Clauer, N., Belcourt, O.,Coulibaly, Y.,
785 Banks, D.A. and Guillocheau, F. 2012. A major Late Jurassic fluid event at the
786 basin/basement unconformity in western France: 40Ar/39Ar and K–Ar dating, fluid
787 chemistry, and related geodynamic context. *Chemical Geology*, **322–323**, 99–120.
788
789 Clerc, C. and Lagabrielle, Y. 2014. Thermal control on the modes of crustal thinning leading
790 to mantle exhumation: Insights from the Cretaceous Pyrenean hot paleomargins. *Tectonics*,
791 **33**, 1340–1359.
792
793 Clerc, C., Lahfid, A., Monié, P., Lagabrielle, Y., Chopin, C., Poujol, M., Boulvais, P.,
794 Ringenbach, J.-C., Masini, E. and de St Blanquat, M. 2015. High-temperature metamorphism
795 during extreme thinning of the continental crust: a reappraisal of the North Pyrenean
796 passive paleomargin. *Solid Earth*, **6**, 643–668.
797
798 Corre, B., Boulvais, P., Boiron, M.C., Lagabrielle, Y., Marasi, L. and Clerc, C. 2018. Fluid
799 circulations in response to mantle exhumation at the passive margin setting in the north
800 Pyrenean zone, France. *Mineralogy Petrology*, **97**, 109-142. DOI: 10.1007/s00710-018-0559-
801 x.
802
803 Courel, L., Ait Salem, H., Benaouiss, N., Et-Touhami, M., Fekirine, B., Ouijidi, M., Soussi, M.
804 and Tourani, A. 2003. Mid-Triassic to Early Liassic clastic/evaporitic deposits over the
805 Maghreb platform. *Paleogeography, Paleoclimatology, Paleoecology*, **196**, 157-176.
806
807 Cruset, D., Cantarero, I., Benedicto, A., John, C. M., Vergés, J., Albert, R., Gerdes, A. and
808 Travé, A. (2020). From hydroplastic to brittle deformation: controls on fluid flow in fold and
809 thrust belts. Insights from the Lower Pedraforca thrust sheet (SE Pyrenees), *Marine*
810 *Petroleum Geology*, **120**, 104517. doi.org/10.1016/j.marpetgeo.2020.104517
811
812 Cugerone, A. 2019. Impact of recrystallisation and metamorphism on the mobility of
813 germanium and related elements in orogenic Pb-Zn deposits: example of the Pyrenean Axial
814 Zone mineralisations (France-Spain). PhD thesis, University of Montpellier, HAL Id: tel-
815 02578708

816

817 Debroas, E.J., Canérot, J. and Bilotte, M. 2010. Les Brèches d'Urdach, témoins de
818 l'exhumation du manteau pyrénéen dans un escarpement de faille Vraconnien-Cénomanien
819 inférieur (zone nord-pyrénéenne, Pyrénées-Atlantiques, France). *Géologie de la France*, **2**,
820 53–63.

821

822 Debure, M., Lassin, A., Marty, N.C., Claret, F., Virgone, A., Calassou, S. and Gaucher, E.C.
823 2019. Thermodynamic evidence of giant salt deposit formation by serpentinisation: an
824 alternative mechanism to solar evaporation. *Scientific reports*, **9**, 1-11.

825

826 Dubessy, J., Geisler, D., Kosztolanyi, C. and Vernet, M. 1983. The determination of sulphate
827 in fluid inclusions using the M.O.L.E. Raman microprobe. Application to a Keuper halite and
828 geochemical consequences. *Geochimica Cosmochimica Acta*, **47**, 1-10.

829

830 Duretz, T., Asti, R., Lagabrielle, Y., Brun, J.P., Jourdon, A., Clerc, C. and Corre, B. 2020.
831 Numerical modelling of syn-rift salt tectonics and mantle exhumation in the Cretaceous
832 Pyrenean Rift. *Basinal Research*, doi.org/10.1111/bre.12389

833

834 Evans, D. A. D. 2006. Proterozoic low orbital obliquity and axial-dipolar geomagnetic field
835 from evaporite palaeolatitudes. *Nature*, **444,** 51–55.

836

837 Fallourd, S., M. Poujol, P. Boulvais, J.-L. Paquette, M. de Saint Blanquat, and P. Rémy 2014. In
838 Situ LA-ICP-MS U–Pb Titanite Dating of Na–Ca Metasomatism in Orogenic Belts: The North
839 Pyrenean Example. *International Journal of Earth Sciences,* **103**, 667–682,
840 doi.org/10.1007/s00531-013-0978-1

841

842 Fanlo, I., Touray, J. C., Subias, I., and Fernadez-Nieto, C. 1998. Geochemical patterns of a
843 sheared fluorite vein, Parzan, Spanish Central Pyrenees. *Mineralium Deposita*, **33**, 620-632.

844

845 Fillon, C., Mouthereau, F., Calassou, S., Pik, R., Bellahsen, N., Gautheron,C., Stockli, D.
846 Brichau, S., Daril, N., Mouchené, M. and Van der Beek, P. 2021. Post-orogenic exhumation in

the western Pyrenees: evidence for extension driven by pre-orogenic inheritance. *Journal Geological Society London*, **178**, doi.org/10.1144/jgs2020-079.

Fontes, J. C. and Matray, J. M. 1993. Geochemistry and origin of formation brines from the Paris Basin, France: 1. Brines associated with Triassic salts. *Chemical Geology*, **109**, 149-175

Ford, M., and Verges J. 2020. Evolution of a salt-rich transtensional rifted margin, Eastern North Pyrenees, France. *Journal of the Geological Society of London*, doi.org/10.1144/jgs2019-157

Gleeson, S.A., Yardley, B.W.D, Munz, I.A., and Boyce, A.J. 2003. Infiltration of basinal fluids into high-grade basement, South Norway: sources and behaviour of waters and brines. *Geofluids*, **3**, 33– 48.

Golberg, J. M., and Maluski H. 1988, Données nouvelles et mise au point sur l'âge du métamorphisme pyrénéen. *Compte-Rendus Académie Sciences*, **306,** 429-435.

Grandia, E., Cardellach, E., Canals, A. and Banks, D.A. 2003a. Geochemistry of the fluids related to epigenetic carbonate-hosted Zn-Pb deposits in the Maestrat Basin, Eastern Spain: fluid inclusion and isotope (Cl, C, O, S, Sr) evidence. *Economic Geology*, **98**, 933-954.

Grandia, F., Canals, A., Cardellach, E., Banks, D.A and Perona, J. 2003b. Origin of ore-forming brines in sediment-hosted Zn-Pb deposits of the Basque-Cantabrian Basin, Northern Spain. *Economic Geology*, **98**, 1397-1411.

Hovland, M., Rueslåtten,H. and Johnsen, H.K. 2018, Large salt accumulations as a consequence of hydrothermal processes associated with 'Wilson cycles': A review, Part 2: Application of a new salt-forming model on selected cases. *Marine Petroleum Geology*, **92**, 128-148.

Incerpi, N., Manatschal, G., Martire, L., Bernasconi, S.M., Gerdes, A. and Bertok, C. 2020. Characteristics and timing of hydrothermal fluid circulation in the fossil Pyrenean

879 hyperextended rift system: new constraints from the Chaînons Béarnais (W Pyrenees).
880 *International Journal of Earth Sciences*, doi.org/10.1007/s00531-020-01852-6.
881
882 Izquierdo-Llavall, E., Menant, A., Aubourg, C., Callot, J.-P., Hoareau, G., Camps, P., Péré, E.
883 and Lahfid, A. (2020) Preorogenic Folds and Syn-Orogenic Basement Tilts in an Inverted
884 Hyperextended Margin: The Northern Pyrenees Case Study. *Tectonics*, **39**, e2019TC005719.
885
886 Jackson, M.P.A. and Talbot, C.J. 1986. External shapes, strain rates, and dynamics of salt
887 structures. *GSA Bulletin*, **97**, 305–323.
888
889 James, V. and Canérot, J. 1999. Diapirisme et structuration post-triasique des Pyrénées
890 occidentales et de l'Aquitaine méridionale (France). *Eclogae Geologica Helvetica*, **92,** 63-72.
891
892 Jammes, S., Manatschal, G. and Lavier, L. 2010. Interaction between prerift salt and
893 detachment faulting in hyperextended rift systems: The example of the Parentis and
894 Mauléon basins (Bay of Biscay and western Pyrenees). *AAPG Bulletin*, **94**, 957–975.
895
896 Jammes, S., Manatschal, G., Lavier, L. and Masini, E. 2009. Tectonosedimentary evolution
897 related to extreme crustal thinning ahead of a propagating ocean: example of the western
898 Pyrenees. *Tectonics,* **28**, TC4012, doi:10.1029/2008TC002406
899
900 Johnson, C.A., Cardellach, E., Tritlla, J. and Hanan, B.B. 1996. Cierco Pb-Zn-Ag vein deposits:
901 Isotopic and fluid inclusion evidence for Formation during the Mesozoic extension in the
902 Pyrenees of Spain. *Economic Geology*, **91**, 497-506.
903
904 Jolivet, M., Labaume, P., Monié, P., Brunel, M., Arnaud, N., and Campani, M. 2007.
905 Thermochronology constraints for the propagation sequence of the South-Pyrenean
906 basement thrust system (France-Spain). *Tectonics,* **26**,
907 http://dx.doi.org/10.1029/2006TC002080.
908

Labaume, A. and Teixell, A. 2020. Evolution of salt structures of the Pyrenean rift (Chaînons Béarnais, France): Form hyperextension to tectonic inversion. *Tectonophysics*, **785**, 228451 doi: 10.1016/j.tecto.2020228451.

Labaume, P., Meresse, F., Jolivet, M., Teixell, A. and Lahfid, A. 2016. Tectonothermal history of an exhumed thrust-sheet-top basin: An example from the south Pyrenean thrust belt. *Tectonics*, **35**, 1280-1313, https://doi.org/10.1002/2016TC004192

Lacroix, B., Buatier, M., Labaume, P., Trave, A., Dubois, M., Charpentier D., Ventalon, S., and Convert-Gaubier, D. 2011. Microtectonic and geochemical characterisation of thrusting in a foreland basin: Example of the South-Pyrenean orogenic wedge (Spain). *Journal of Structural Geology*, **33**, 1359-1377.

Lagabrielle, Y., Asti, R., Fourcade, S., Corre, B., Poujol, M., Uzel, J., Labaume, P., Clerc, C., Lafay, R., Picazo, S. and Maury, R. 2019a. Mantle exhumation at magma-poor passive continental margins. Part I. 3D architecture and metasomatic evolution of a fossil exhumed mantle domain (Urdach lherzolite, north-western Pyrenees, France). *Bulletin de la Société Géologique de France*, **190**, 8. doi.org/10.1051/bsgf/2019007

Lagabrielle, Y., Asti, R., Fourcade, S., Corre, B., Uzel, J., Labaume, P., Clerc, C., Lafay, R. and Picazo S. 2019b. Mantle exhumation at magma-poor passive continental margins. Part II. Tectonic and metasomatic evolution of large-displacement detachment faults preserved in a fossil distal margin domain (Saraillé lherzolites, north-western Pyrenees, France). *Bulletin de la Société Géologique de France*, **190**,14. doi.org/10.1051/bsgf/2019013

Lagabrielle, Y., Asti, R., Duretz, T., Clerc, C., Fourcade, S., Teixell, A., Labaume, P., Corre, B. and Saspiturry, N. 2020. A review of cretaceous smooth-slopes extensional basins along the Iberia-Eurasia plate boundary: How pre-rift salt controls the modes of continental rifting and mantle exhumation. *Earth Science Reviews*, **201**, 103071. doi.org/10.1016/j.earscirev.2019.103071

940 Leleu, S., Hartley, A., vanOosterhout, C., Kennan, L., Ruckwied,K. and Gerdes, K. 2016.
941 Structural, Stratigraphic and sedimentological characterisation of a wide rift system: The
942 Triassic rift system of the Central Atlantic Domain. *Earth Science Reviews*,
943 doi:10.1016/j.earscirev.2016.03.008
944
945 Levet, S., Toutain, J. P. , Munoz, M., Berger, G., Negrel, P., Jendrzejewski, N., Agrinier, P.
946 and Sortino, F. 2002. Geochemistry of the Bagnères-de-Bigorre thermal waters from the
947 North Pyrenean Zone (France). *Geofluids*, https://doi.org/10.1046/j.1468-8123.2002.00030.x
948
949 Martz, P., Mercadier, J., Cathelineau, M., Boiron, M.C., Quirt, D., Doney, A., Gerbeaud, O., De
950 Wally, E. and Ledru, P. 2019. Formation of U-rich mineralising fluids through basinal brine
951 migration within basement-hosted shear zones: A large-scale study of the fluid chemistry
952 around the unconformity-related Cigar Lake U deposit (Saskatchewan, Canada). *Chemical*
953 *Geology*, **508**, 116-143.
954
955 Masini, E., Manatschal, G., Tugend, J., Mohn, G. and Flament, J.-M. 2014. The tectono-
956 sedimentary evolution of a hyper-extended rift basin: the example of the Arzacq–Mauléon
957 rift system (Western Pyrenees, SW France). *International Journal of Earth Sciences*, **103**,
958 1569–1596. https://doi.org/10.1007/s00531-014-1023-8
959
960 McCaig, A.M., Wayne, D.M., Marshall, J.D., Banks,D.A. and Henderson, I., 1995. Isotopic
961 and fluid inclusion studies of fluid movement along the Gavarnie Thrust, central Pyrenees;
962 reaction fronts in carbonate mylonites. *American Journal of Science*, 295, 309-343
963
964 McCaig, A.M., Tritlla, J. and Banks, D.A. 2000. Fluid mixing and recycling during Pyrenean
965 thrusting: Evidence from fluid inclusion halogen ratios. *Geochimica Cosmochimica Acta*, **64**,
966 3395-3412.
967
968 Meresse, F. 2010. Dynamique d'un prisme orogénique intracontinental : évolution
969 thermochronologique (traces de fission sur apatite) et tectonique de la Zone Axiale et des
970 piémonts des Pyrénées centro-occidentales. PhD thesis , Montpellier II Univ., 277 p.
971

Montigny, R., Azambre, B., Rossy, M., and Thuizat, R. 1986. K-Ar study of cretaceous magmatism and metamorphism in the pyrenees: age and length of rotation of the iberian peninsula. *Tectonophysics*, **129,** 257-213.

Motte, G., Hoareau, G., Callot, J.P., Révillon, S., Piccoli, F., Calassou, S. and Gaucher, E.C. 2021. Rift and salt-related multi-phase dolomitisation: example from the northwestern Pyrenees. *Marine Petroleum Geology,* doi.org/10.1016/j.marpetgeo.2021.104932

Mouthereau, F., Filleaudeau,P.Y., Vacherat,A., Pik, R., Lacombe, O., Fellin, M.G., Castelltort, S., Christophoul, F. and Masini, E. 2014. Placing limits to shortening evolution in the Pyrenees: role of margin architecture and implications for the Iberia/Europe convergence. *Tectonics,* **33**,2283-2314. doi:10.1002/2014TC003663.

Munoz, M., Baron, S., Boucher, A., Beziat, D. and Salvi S. 2015. Mesozoic vein-type Pb–Zn mineralisation in the Pyrenees: Lead isotopic and fluid inclusion evidence from the Les Argentières and Lacore deposits. *Compte-Rendus Geosciences*, **348**, 322-332.

Nalpas, T. and Brun, J.P. 1993. Salt flow and diapirism related to extension at crustal scale. *Tectonophysics*, **228**, 349-362.

Nteme Mukonzo, J., Boiron, M.C., Lagabrielle, Y., Cathelineau, M. and Quesnel B. 2021. Fluid-rock interactions along detachment faults during continental rifting and mantle exhumation: the case of the Urdach lherzolite body (North-Pyrenees). *Journal of the Geological Society of London*, doi.org/10.1144/jgs2020-116.

Olivet, J.L. 1996. La cinématique de la plaque ibérique. *Bulletin des Centres de Recherche Exploration Production Elf Aquitaine*, **20**, 131–195.

Orti, F., Perez-Lopez, A. and Salvany, J.M. 2017. Triassic evaporites of Iberia: Sedimentological and palaeogeographical implications for the western Neotethys Evolution during the Middle Triassic–Earliest Jurassic. *Palaeogeography Palaeoclimatology Palaeoecology*, **471**, 157–180.

Parseval, de P. 1992. Étude minéralogique et géochimique du gisement de talc et chlorite de Trimouns, Ph. D. thesis, Université de Toulouse III.

Poujol, M., Boulvais, P., Kosler, J. 2010. Regional-scale Cretaceous albitisation in the Pyrenees: evidence from in situ U-Th-Pb dating of monazite, titanite and zircon. *Journal of the Geological Society of London*, **167**, 751-767. doi.org/10.1144/0016-76492009-144

Quesnel, B., Boiron, M.C., Cathelineau, M., Truche, L., Rigaudier, T., Bardoux, G., Agrinier, P., de Saint Blanquat, M., Masini, E. and Gaucher, E.C. 2019. Nature and origin of mineralizing fluids in hyper-extensional systems, the case of Cretaceous Mg-metasomatism in the Pyrenees. *Geofluids*, doi.org/10.1155/2019/7213050

Rahl, J.M., Haines, S.H. and van der Pluijm, B.A. 2011. Links between orogenic wedge deformation and erosional exhumation: Evidence from illite age analysis of fault rock and detrital thermochronology of syn-tectonic conglomerates in the Spanish Pyrenees. *Earth and Planetary Science Letters,* **307**, 180–190.

Renard, S., Pironon, J., Sterpenich, J., Carpentier, C., Lescanne, M. and Gaucher, E. C. 2019. Diagenesis in Mesozoic carbonate rocks in the North Pyrenees (France) from mineralogy and fluid inclusion analysis: example of Rousse reservoir and caprock. *Chemical Geology*, **508**, 30-46. https://doi.org/10.1016/j.chemgeo.2018.06.017

Richard, A., Boulvais, P., Mercadier, J., Boiron, M.C., Cathelineau, M., Cuney M. and France - Lanord, C. 2013. From evaporated seawater to uranium mineralising brines: Isotopic and trace element study of quartz dolomite veins in the Athabasca system. *Geochimica Cosmochimica Acta,* **113**, 38-59.

Ryan, W. B.F. 2008. Modeling the magnitude and timing of evaporative draw down during the Messinian salinity crisis. *Stratigraphy*, **5**, 227-243

Salardon, R., Carpentier, C., Bellahsen, N., Pironon, J. and France-Lanord, C. 2016. Interactions between tectonics and fluid circulations in an inverted hyper-extended basin: Example of mesozoic carbonate rocks of the western North Pyrenean Zone (Chaînons Béarnais, France). *Marine Petroleum Geology*, doi: 10.1016/j.marpetgeo.2016.11.018.

Sanchez, V., Vindel, E., Martin-Crespo, M., Corbella, M., Cardellach, E. and Banks D.A. 2009. Sources and composition of fluids associated with fluorite deposits of Asturias (N Spain). *Geofluids,* **9**, 338-355.

Sanchez, V., Cardellach, E., Corbella, M., Vindel, E., Martin-Crespo, M. and Boyce, A.J. 2010. Variability in fluid sources in the fluorite deposits from Asturias (N Spain): Further evidences from REE, radiogenic (Sr, Sm, Nd) and stable (S, C, O) isotope data. *Ore Geology Reviews*, doi : 10.1016/j.oregeorev.2009.12001.

Saspiturry, N., Lahfid, A., Baudin, T., Guillou-Frottier, L., Razin, P., Issautier B., Le Bayon, B., Serrano, O., Lagabrielle, Y. and Corre, B. 2020. Paleogeothermal gradients across an inverted hyperextended rift system: Example of the Mauléon fossil rift (Western Pyrenees). Tectonics, doi: 10.17632/47kgv7r9wm.3.

Saura, E., L. Ardèvol i Oró, A. Teixell, and J. Vergés (2016) Rising and falling diapirs, shifting depocenters, and flap overturning in the Cretaceous Sopeira and Sant Gervàs subbasins (Ribagorça Basin, southern Pyrenees), *Tectonics*, **35**, 638–662, doi: 10.1002/2015TC004001.

Schärer, U., de Parseval, P., Polvé, M. and de Saint Blanquat, M. 1999. Formation of the Trimouns talc-chlorite deposit (Pyrenees) from persistent hydrothermal activity between 112 and 97 Ma. *Terra Nova*, **11**, 30–37.

Scribano, V., Carbone, S., Manuella, F.C., Hovland, M., Rueslatten , H. and Johnsen, H.K. 2017. Origin of salt giants in abyssal serpentinite systems. *International Journal of Earth Sciences,* **106**, 2595-2608.

1066 Shao H., Wang, Y., Kolditzc O., Nagelc T. and Brüningad T. 2019. Approaches to multi-scale
1067 analyses of mechanically and thermally-driven migration of fluid inclusions in salt rocks.
1068 *Physics and Chemistry of the Earth*, **113**, 1-13. doi.org/10.1016/j.pce.2019.07.003
1069
1070 Souche, A., Dabrowski, M., Andersen, T.B. 2014. Modeling thermal convection in
1071 supradetachment basins: example from western Norway. *Geofluids*, **14**, 58-74.
1072
1073 Spiers, C.J., Schutjens, P.M.T.M., Brzesowsky, R.H., Peach, C.J., Liezenberg, J.L. and Zwart,
1074 H.J. 1990. Experimental determination of constitutive parameters governing creep of rock
1075 salt by pressure solution. In: Knipe, R.J. and Rutter, E.H. (eds), *Deformation Mechanisms,*
1076 *Rheology and Tectonics. Geological Society Special Publication*, **45**, 215-227.
1077
1078 Steele-MacInnis, M., Bodnar, R.J. and Naden, J. 2011. Numerical model to determine the
1079 composition of H_2O-NaCl-$CaCl_2$ fluid inclusions based on microthermometric and
1080 microanalytical data. *Geochimica Cosmochimica Acta*, **75**, 21–40.
1081
1082 Stober, I. and Bucher, K. 2004. Fluid sinks within the earth's crust. *Geofluids*, **4**, 143-151
1083
1084 Subias, I. and Fernandez-Nieto C. 1995. Hydrothermal events in the Valle de Tena (Spanish
1085 Western Pyrenees) as evidenced by fluid inclusions and trace-element distribution from
1086 fluorite deposits. *Chemical Geology*, **124**, 267-282.
1087
1088 Subias, I., Fanlo, I., and Billström, K. 2015. Ore-forming timing of polymetallic-fluorite low
1089 temperature veins from Central Pyrenees: A Pb, Nd and Sr isotope perspective. *Ore Geology*
1090 *Reviews,* **70**, 241-251.
1091
1092 Teixell, A., Labaume, P., Ayarza, P., Espurt, N., de Saint Blanquat, M. and Lagabrielle, Y. 2018.
1093 The present-day and past crustal structure of the Pyrenean-Cantabrian belt: a review and
1094 new interpretations from recent concepts and data. *Tectonophysics,* **724-725**, 146-170. DOI:
1095 10.1016/j.tecto.2018.01.009.
1096

Teixell, A. 1996. The Anso´ transect of the southern Pyrenees: basement and cover thrust geometries. *Journal of the Geological Society of London*, **153**, 301–310.

Teixell, A., Labaume, P. and Lagabrielle, Y. 2016. The crustal evolution of the west-central Pyrenees revisited: inferences from a new kinematic scenario. *Compte-Rendus Geosciences*, **348**, 257- 267. doi: 10.1016/j.crte.2015.10.010.

Trincal, V., Lanari, P., Buatier, M., Lacroix, B., Charpentier, D., Labaume, P. and Munoz, M. 2015. Temperature micro-mapping in oscillatory-zoned chlorite: Application to study of a green-schist facies fault zone in the Pyrenean Axial Zone (Spain). *American Mineralogist*, **100**, 2468-2483.

Trincal, V., Buatier, M., Charpentier, D., Lacroix, B., Lanari, P., Labaume, P., Lahfid, A., and Vennemann, T. 2017. Fluid–rock interactions related to metamorphic reducing fluid flow in meta- sediments: example of the Pic- de- Port- Vieux thrust (Pyrenees, Spain). *Contributions to Mineralogy and Petrology*, **172**, 78, DOI 10.1007/s00410-017-1394-5.

Tugend, J., Manatschal, G., Kusznir, N.J., Masini, E., Mohn, G., and Thinon, I. 2014. Formation and deformation of hyperextended rift systems: Insights from rift domain mapping in the Bay of Biscay-Pyrenees. *Tectonics*, **33**, 1239–1276. https://doi.org/10.1002/2014TC003529

Turner, P. and Sherif, H.,2007. A giant Late Triassic – Early Jurassic evaporitic basin on Saharan platform, North Africa. In Evaporites through space and time, *Geological Society of London, Special Publications*, **28**5, 87-105.

Urai, J.L., Spiers, C.J., Zwart., H.J. and Lister, G.S. 1986. Weakening of rock salt by water during long-term creep. *Nature,* **324**, 554-557.

Urai, J.L., Schleder, Z., Spiers, C.J. and Kukla, P.A. 2008. Flow and transport properties of saltrocks. In: Littke, R., Bayer, U., Gajewski, D., Nelskamp, S., editors. *Dynamics of complex intracontinental basins: The Central European Basin System*. Berlin, Springer, 277–90.

Vacherat, A., Mouthereau, F., Pik, R., Bernet, M., Gautheron, C., Masini, E., Le Pourhiet, L., Tibaric, B., and Lahfid, A. 2014. Thermal imprint of rift-related processes in orogens as recorded in the Pyrenees. *Earth and Planetary Science Letters*, **408**, 296–306.

Vacherat, A., Mouthereau, F., Pik, R., Bellahsen N., Gautheron, C., Bernet, M., Daudet M., Balansa J., Tibari B., Pina Jamme R., Radal J. 2016. Rift-to-collision transition recorded by tectonothermal evolution of the northern Pyrenees. *Tectonics*, **35**, 907-933, https://doi.org/10.1002/2015TC004016

Vendeville, B.C., Ge, H. and Jackson, P.A. (1995). Scale models of salt tectonics during basement-involved extension. *Petroleum Geosciences*, **1**, 179-183.

Vissers, R.L.M., Ganerod, M., Pennock, G.N. and Van Hinsbergen, D.J.J. 2020. Eocene seismogenic reactivation of a Jurassic ductile shear zone at Cap de Creus, Pyrenees, NE Spain. *Journal of Structural Geology*, **134**, 103994.

Walter, B.F., Burisch, M. and Markl, G. 2016. Long-term chemical evolution and modification of continental basement brines - a field study from the Schwarzwald, SW Germany. *Geofluid,* **16**, 604–623. http://dx.doi.org/10.1111/gfl.12167.

Van Keken, P. E., Spiers, C.J., van den Berg, A.P. and Muyzert, E.J. 1993. The effective viscosity of rock salt: implementation of steady-state creep laws in numerical models of salt diapirism. *Tectonophysics,* **225**, 457-476, https://doi.org/10.1016/0040-1951(93)90310-G

Wayne, D.M. and McCaig, A. M. 1998. Dating fluid flow in shear zones: Rb-Sr and U-Pb studies of syntectonic veins in the Néouvielle Massif, Pyrenees. *Geological Society of London Special Publications*, **144**, 129-135. DOI: 10.1144/GSL.SP.1998.144.01.09

Figure captions

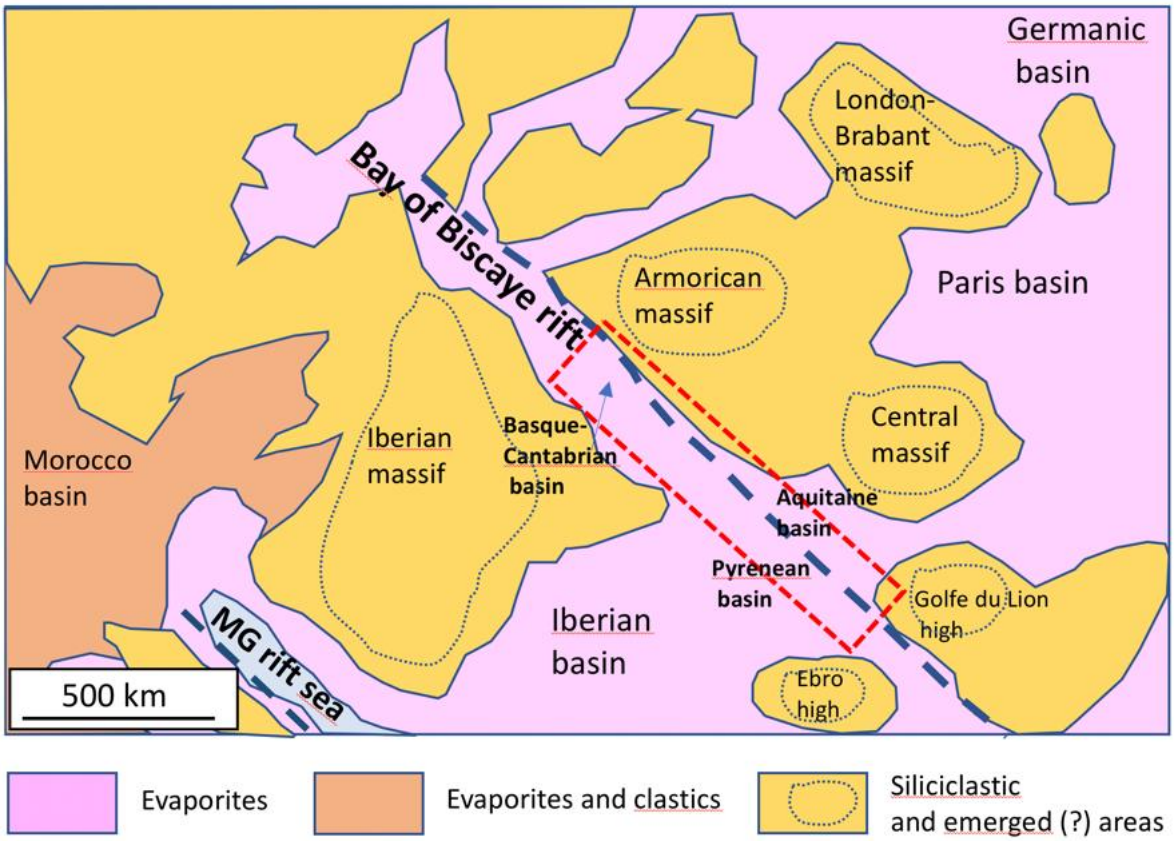

Fig. 1: Distribution of predominant Triassic evaporites (in pink) in southern Europe with an indication of the Pyrenean area from a palaeogeographic map for late Triassic slightly modified from Orti et al. (2017); MG: Maghrebian-Gibraltar.

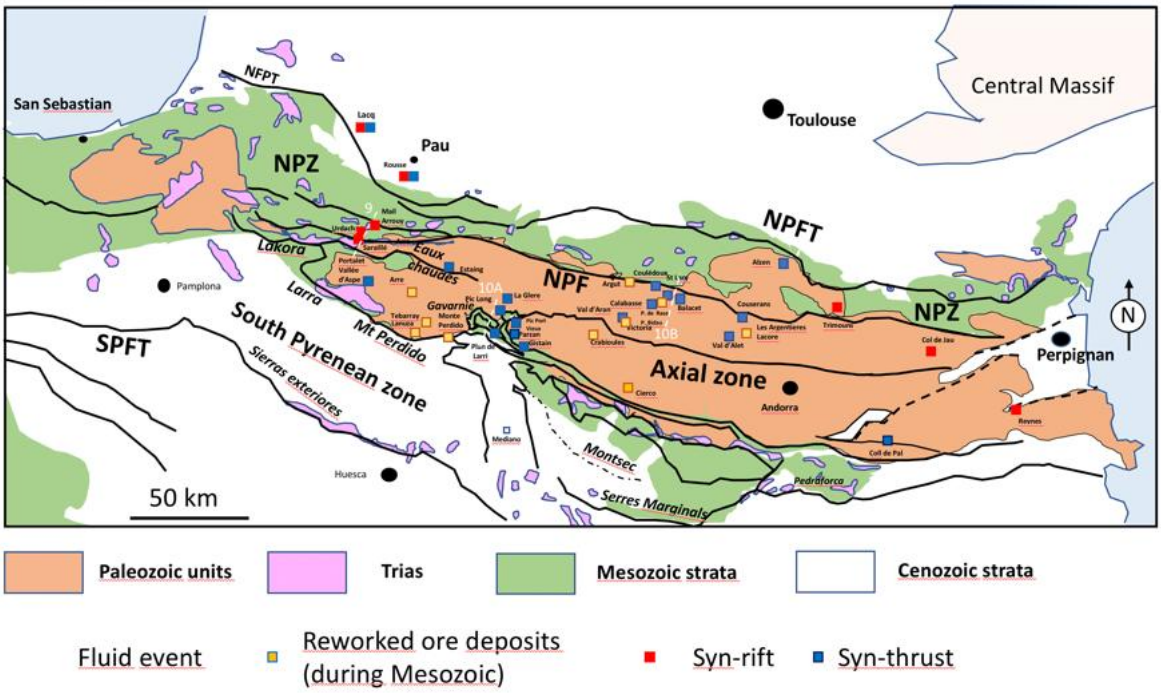

1167

1168

1169 Fig. 2: Distribution of the studied localities in the Pyrenees chain reported on a geological
1170 map modified from Ford and Verges (2020). Red points correspond to localities for which
1171 new data have been acquired during the present work. White circles with a red dot
1172 correspond to localities described in the literature. NPF: North Pyrenean Fault, NPFT: North
1173 Pyrenean Frontal Thrust, SPFT: South Pyrenean Frontal Thrust. The approximative locations
1174 of the cross-section shown in Fig. 9, 10A and 10B are indicated as white dashed lines.

1175

1176 Fig. 3: Macroscopic features of studied samples: A: silicified breccia from basement/ Trias
1177 interface (Urdach, Chaînons Bearnais). B: dolomite cemented breccia in Mano formation
1178 (Mail Arrouy, Chaînons Bearnais); C: prismatic quartz embedded in calcite, from Mg-
1179 metasomatic zone (Col de Jau, eastern Axial zone); D: euhedral bi-terminated quartz prism
1180 on dolomite and talc from Mg-metasomatic zone (Trimouns, Saint Barthelemy massif).

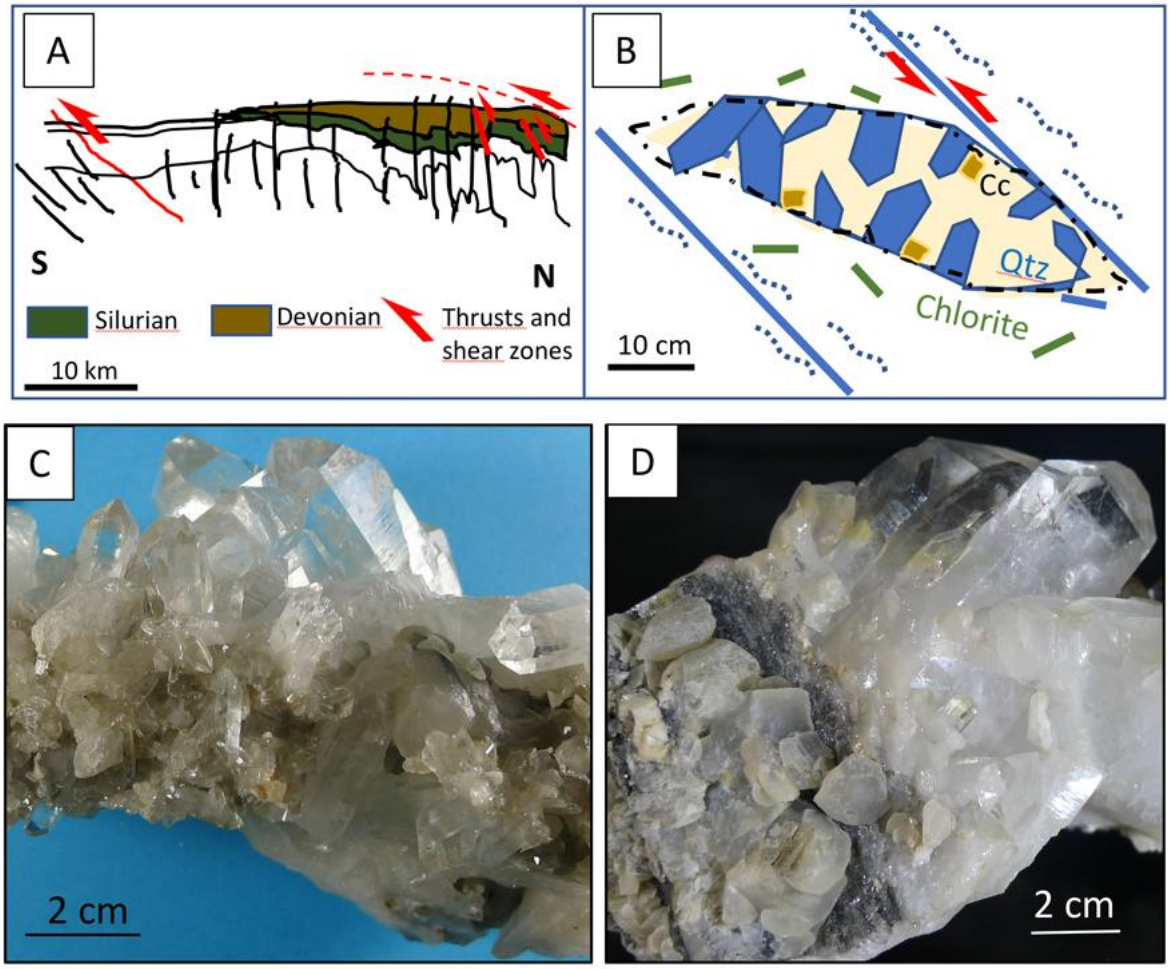

Fig. 4: A: Simplified cross-section of Ariège/ Haute Garonne region close to the North Pyrenean Fault (NPF, see Fig. 2). B; Schematic cross-section of a tension gash developed in relation with reactivated shear planes. Qtz: quartz, CC: calcite; C: Macroscopic features of euhedral quartz from Val d'Alet (Ariège, Axial zone); D: euhedral quartz from Balacet (Ariège, Axial zone).

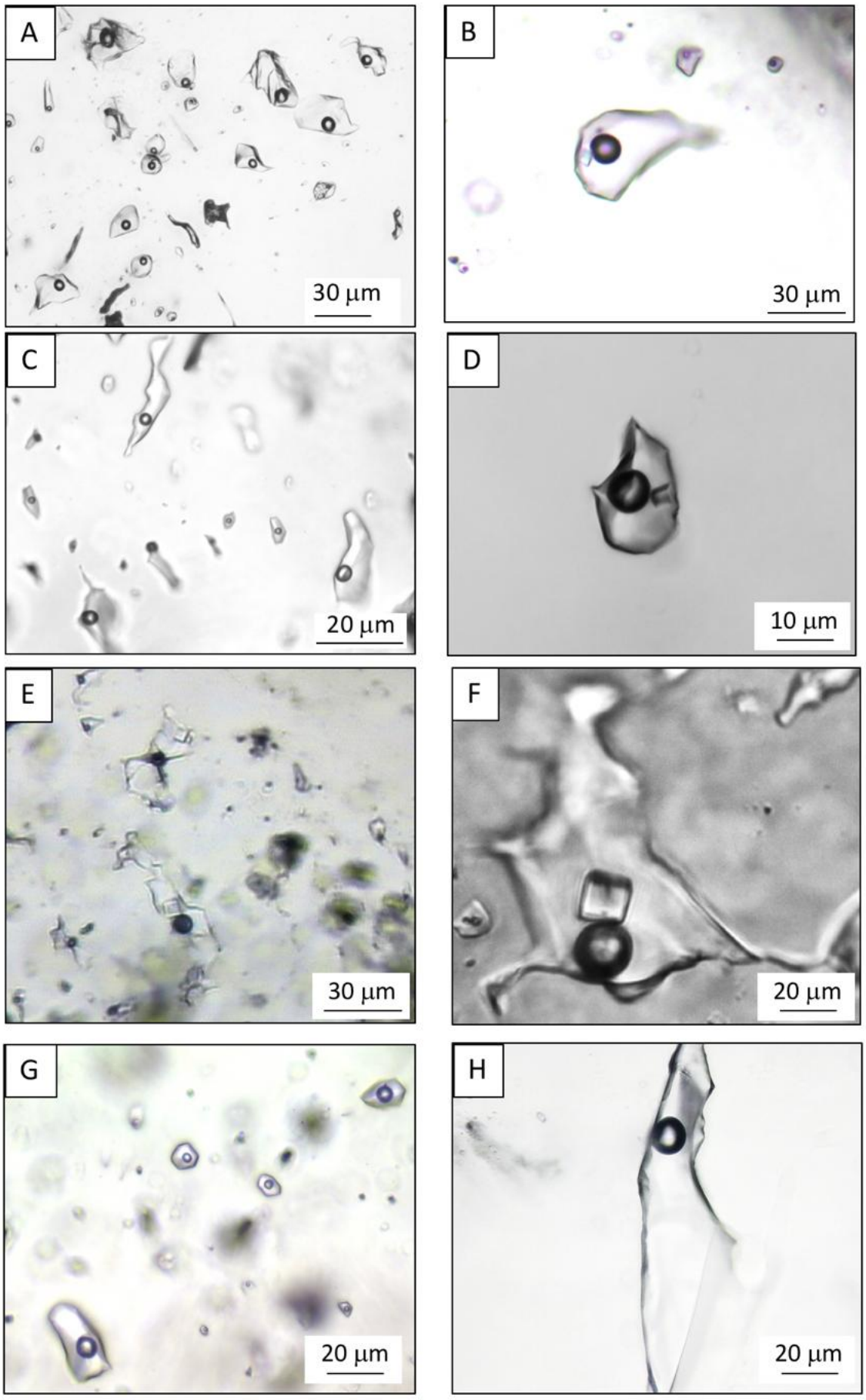

1187

Fig. 5: Fluid inclusion types: A: two-phase fluid inclusions (Lw Fis) from Val d'Alet quartz; B: three-phase fluid inclusion with a halite cube (Lwh Fi) from Val d'Alet quartz; C: two-phase fluid inclusions (Lw Fis) from La Calabasse; D: three-phase fluid inclusions (Lwh Fi) from La Calabasse; E: three-phase fluid inclusions (Lwh Fis) from Col de Jau; F: three-phase fluid inclusion with a halite cube from Etche, Urdach massif (Lwh Fi); G: two-phase fluid inclusions from St Lary (Lw Fis); H: two-phase fluid inclusion (Lw) from Val d'Aran.

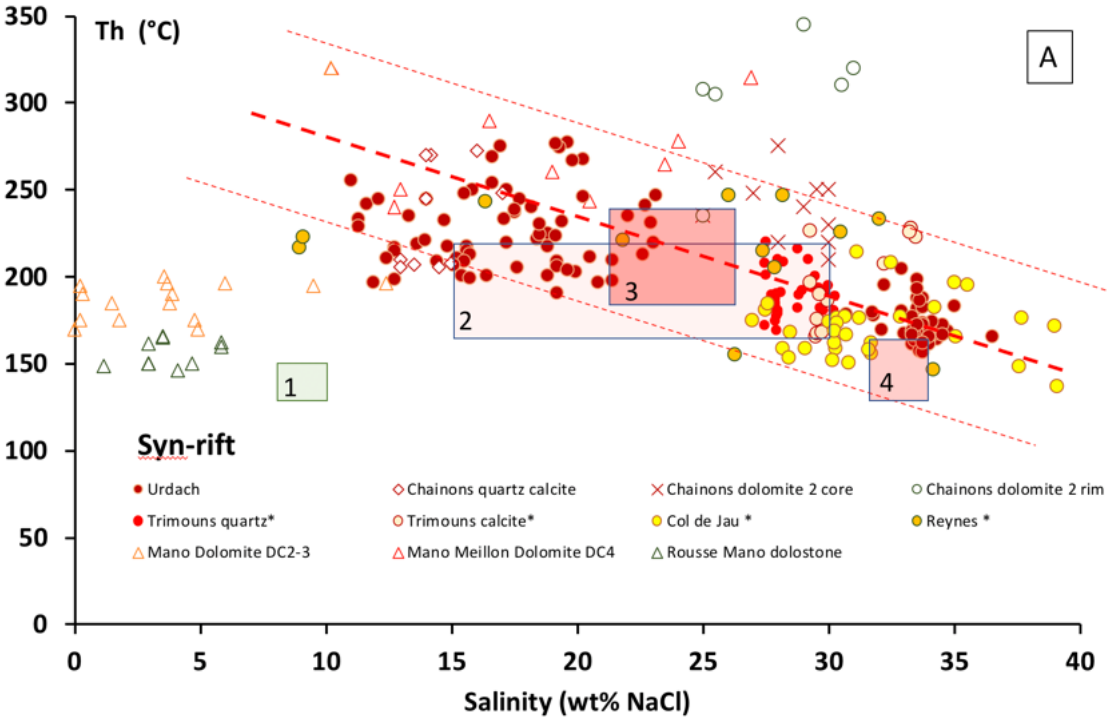

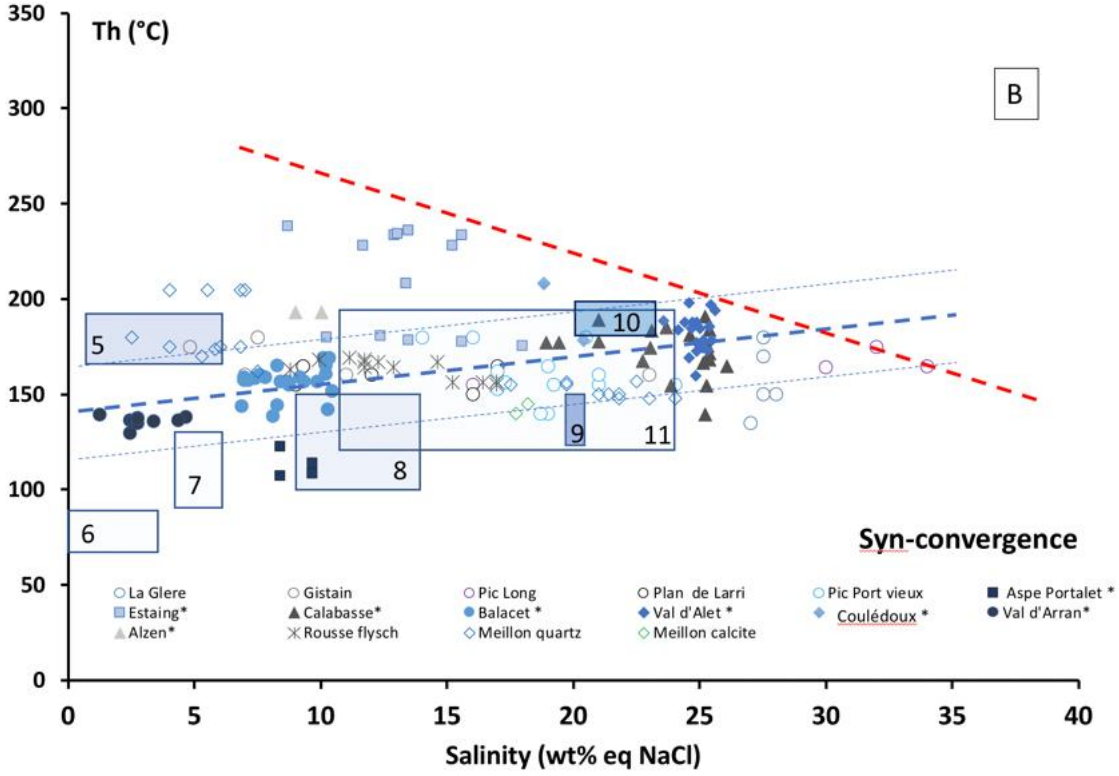

1195

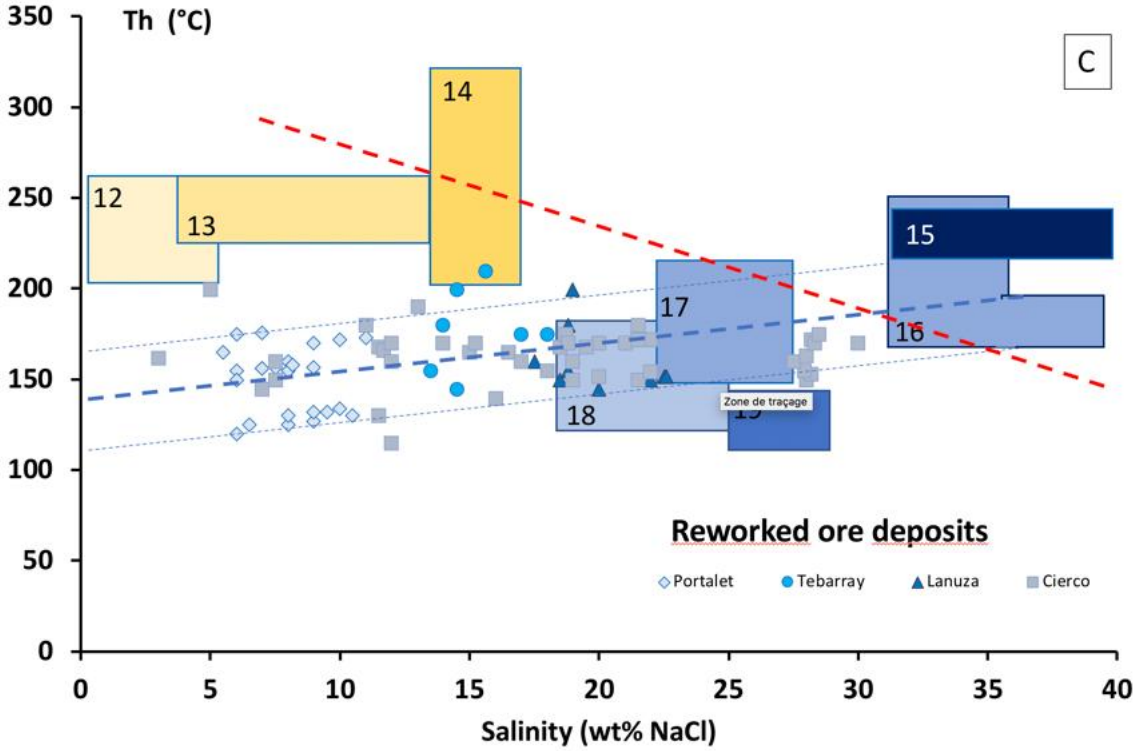

1196

1197

1198 Fig. 6: Synthetic Tm-Th plot of fluid inclusion data for Mesozoic and syn-rift (A), syn-thrust

1199 paleofluids (B) events, and reworked ore deposits (C). Full coloured symbols correspond to

new data (noted with *) and other symbols to literature data. When salinity-Th pairs are lacking, domains have been drawn using ranges and modes given by the authors. Dashed lines indicate main mixing trends, red: syn-rift stage, blue: syn-convergence stage.

Literature data: 1 – Deep Lacq (saddle dolomite, Bahnan, 2019), 2 - Saraille calcite, 3 - Saraille dolomite, 4 - Saraille quartz, Corre et al. , (2018) ; 5-Monte Perdido, Lacroix et al. (2011); 6 – Upper Lacq, dolomite, 7 - Deep Lacq, Anhydrite, 8 - Deep Lacq calcite, Bahnan (2019) ; 9 - Coll de Pal, Canals et al. (1999) ; 10- Parzan quartz, 11 – Parzan fluorite, Fanlo et al. (1998); 12-Pale de Rase, 13- Argut, 14- Pale de Bidau, 15- Victoria 16- Crabioules, 17- Arre, Cugerone, (2019); 18- Lacore, 19- Les Argentières, Munoz et al. (2015); Other data points concern the following localities: Rousse (Renard et al., 2019), Gavarnie thrust (Gistain, Pic de Larri, Pic Port Vieux, Pic Long and La Glere, Mc Caig et al., 2000), Portalet, Tebarray and Lanuza (Subias and Fernandez Nieto, 1995), Cierco (Johnson et al., 1996). Urdach (Nteme Mukonzo et al., 2021), Chainons Bearnais (Chainons., calcite quartz and dolomite, Salardon et al., 2016).

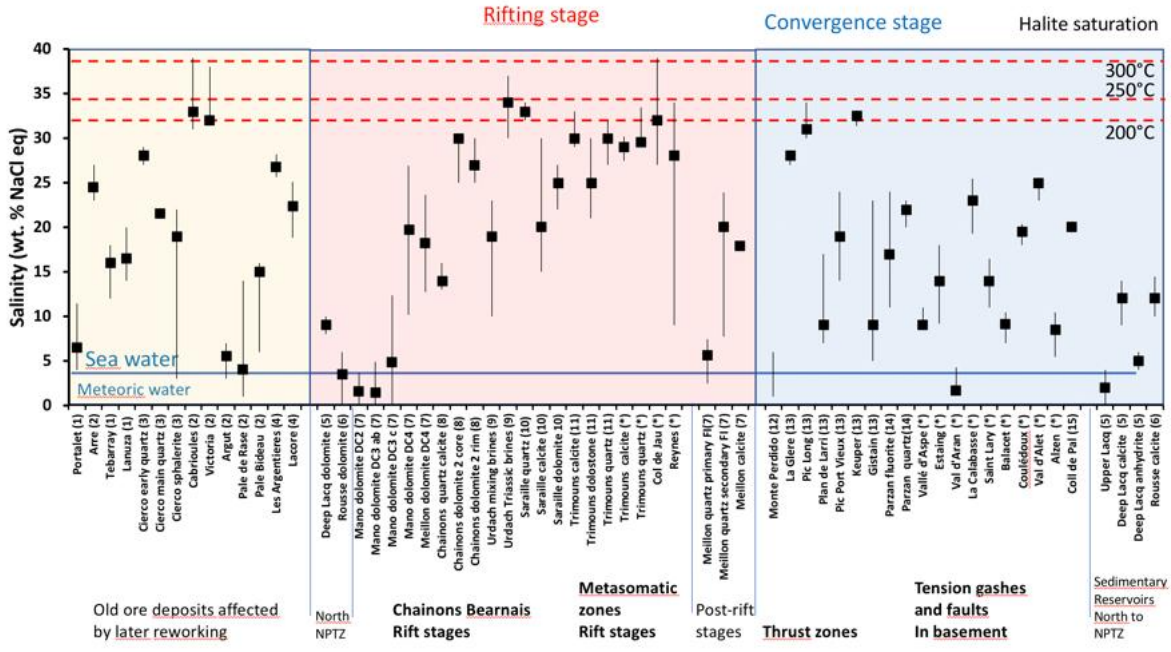

Fig 7: Salinity ranges for all localities, with the indication of halite saturation values and seawater salinity. Data are presented in three groups: reworked ore deposits during post-Triassic, syn-rift fluid stages, and late fluid circulations attributed to thrusts. SW: seawater. References for literature data : 1: Subias and Fernandez Nieto (1995); 2: Cugerone (2019); 3: Johnson et al. (1996) ; 4: Munoz et al. (2015) ; 5: Bahnan (2019); 6 : Renard et al. (2019); 7 : Motte et al. (2021) ; 8 : Salardon et al. (2016); 9 : Nteme Mukonzo et al. (2021); 10 : Corre

et al. (2018); 11: Quesnel et al. (2019) ; 12: Lacroix et al. (2011); 13: McCaig et al. (2000) ; 14: Fanlo et al. (1998); 15: Canals et al. (1999).

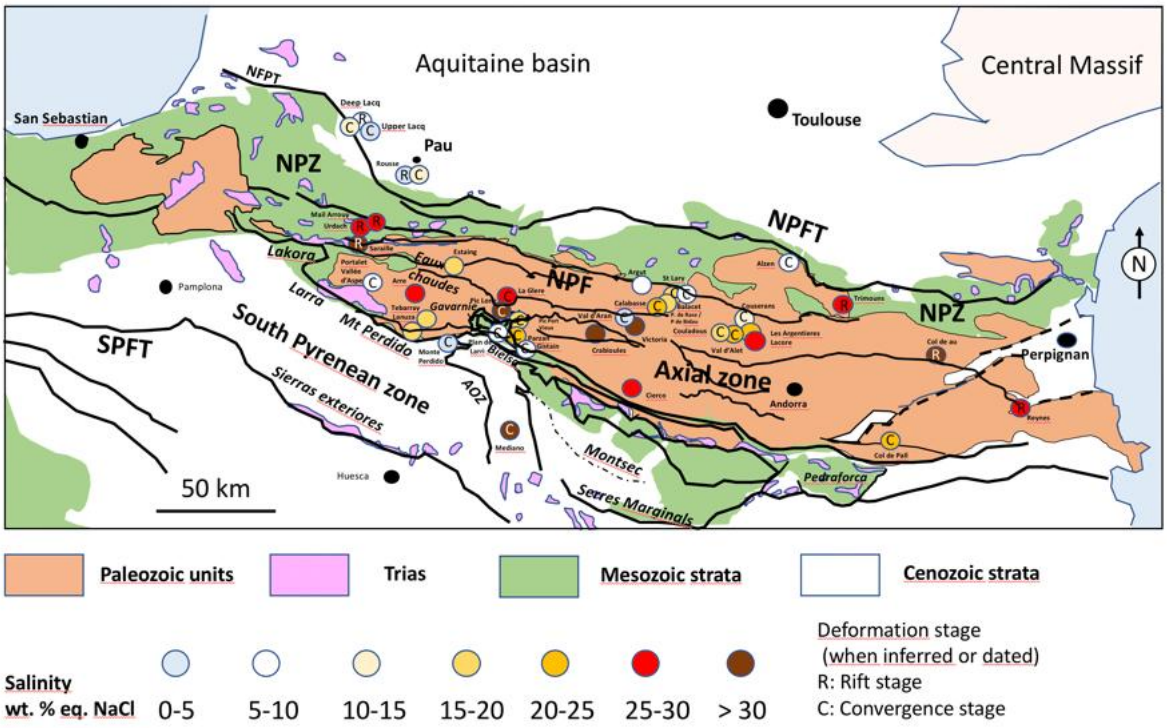

Fig. 8: Map of distribution of salinities of palaeofluids found in newly formed minerals in fractures at the scale of Pyrenees, with an indication of outcropping Upper Trias, major faults and thrust (NFPT North Pyrenean Frontal Thrust, NPF: North Pyrenean Fault). C in circles for localities attributed to syn-convergence events.

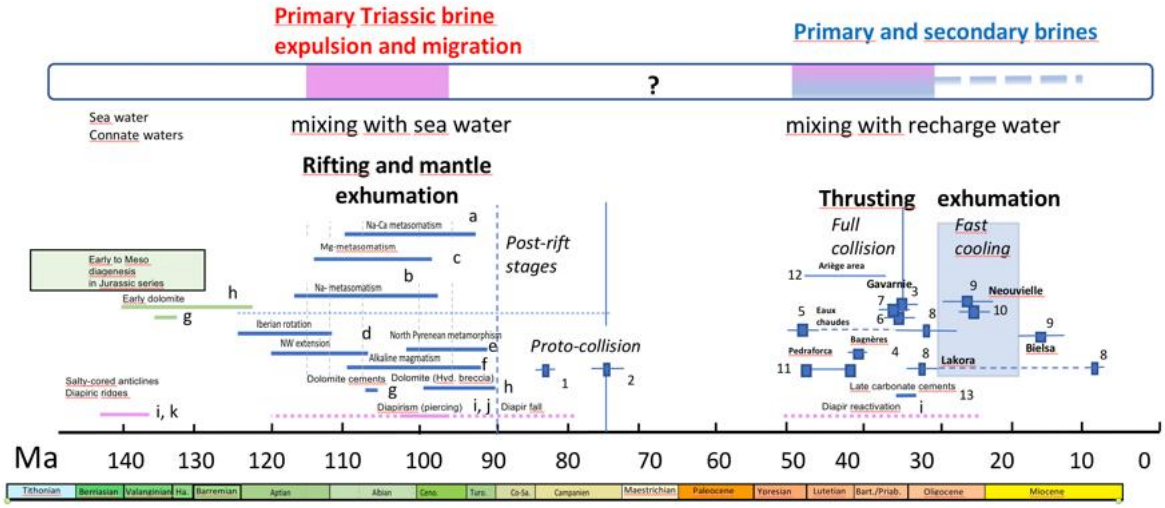

Fig. 9: Main periods of brine migration in the Pyrenees during Mesozoic and Cenozoic. Ages are issued from literature: **Rifting stage** - a: Fallourd et al. (2014); b: Schärer et al. (1999), Boutin et al. (2016); c: Poujol et al. (2010), Boutin et al. (2016); d: Jammes et al., (2010); e:

Olivet (1996); f: Goldberg and Maluski (1988); g: Montigny et al. (1986); g : Motte et al. (2021), h : Incerpi et al. (2020); i : Canérot et al. (2005) ; j : Saura et al. (2015) ; k : James et Canérot (1999) - **Thrusting and exhumation stages** - 1: Vacherat et al. (2014); 2: Mouthereau et al. (2014); 3: Teixell (1996); 4: Meresse (2016); 5: Wayne and McCaig (1998); 6: Rahl et al. (2011); 7: Jolivet et al. (2007) for Gavarnie; 8: Bosch et al. (2016); 9: Jolivet et al. (2007) for Neouvielle area, 10 : Labaume et al. (2016), 11 : Cruset et al., 2020, 12 : Vacherat et al., 2016; 13 : Renard et al., 2019.

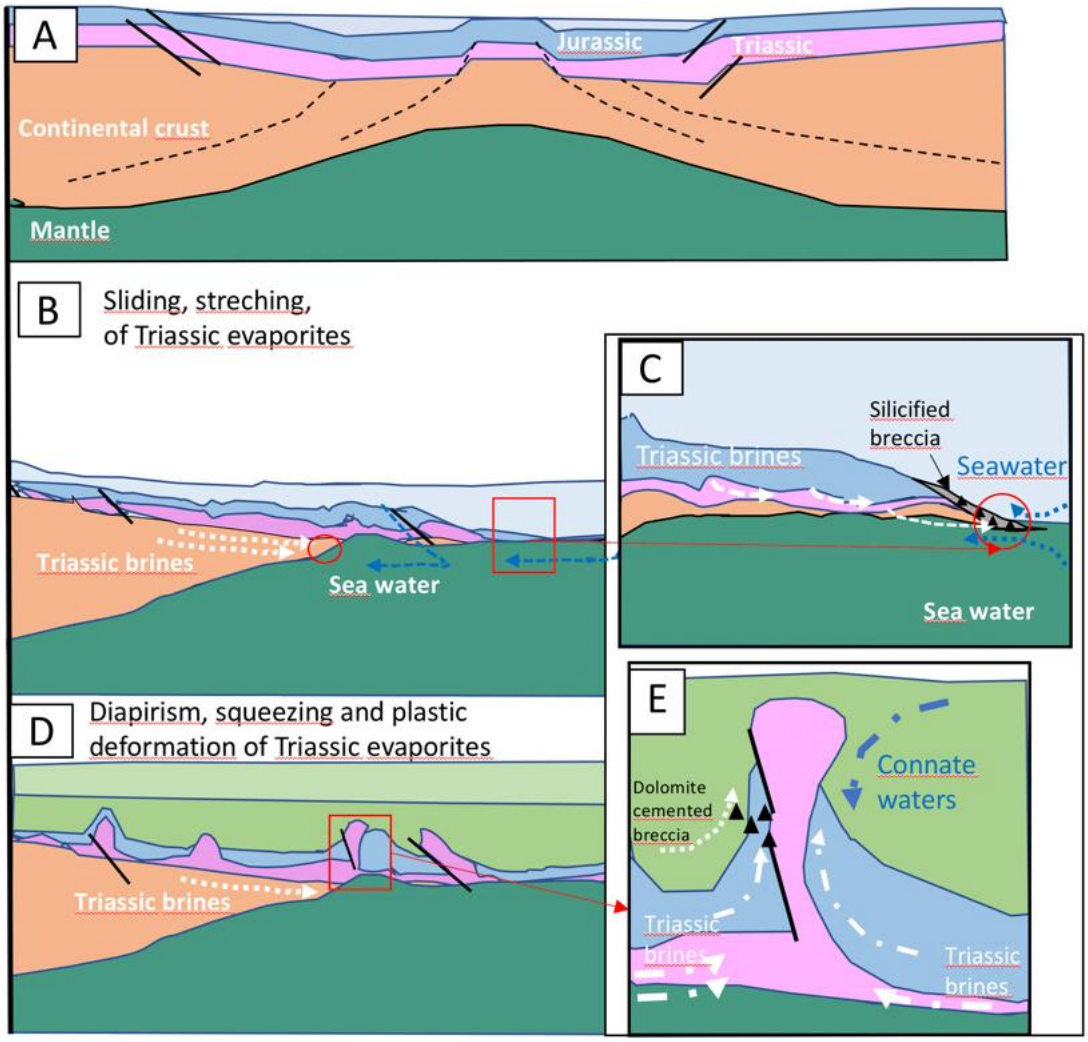

Fig. 10: Conceptual model of fluid circulation. A: pre-extension stage (A) shown to emphasise the continuous cover of a thick evaporite bearing Triassic series before the deformation; B and C: the mid-Cretaceous extensional stage followed by and the diapir piercing stage (simplified cross-sections modified from Teixell et al. (2016) and Duretz et al. (2020)). C: Triassic brines migrate at the boundary between the Paleozoic basement and sedimentary

cover and mix in highly deformed zones corresponding to the mantle sedimentary cover interface. They mix with seawater heated at depth and have interacted with mantle rocks (serpentinisation process). The mixing is anisothermal as the seawater trajectories above the thermal anomalies linked to the mantle uplift are far more heated than brines (anisothermal mixing from Fig. 6A). A temperature drop during mixing yield quartz cementation of hydraulic breccia (as shown in the Urdach example by Nteme Mukonzo et al., 2021). D and E: fluids are issued from further squeezing of evaporites during diapirism stimulated by deformation and faulting (Canérot et al., 2004). Triassic brines may mix with several kinds of fluids (seawater, connate waters), as proposed by Motte et al. (2021) on the example of Mail Arrouy area.

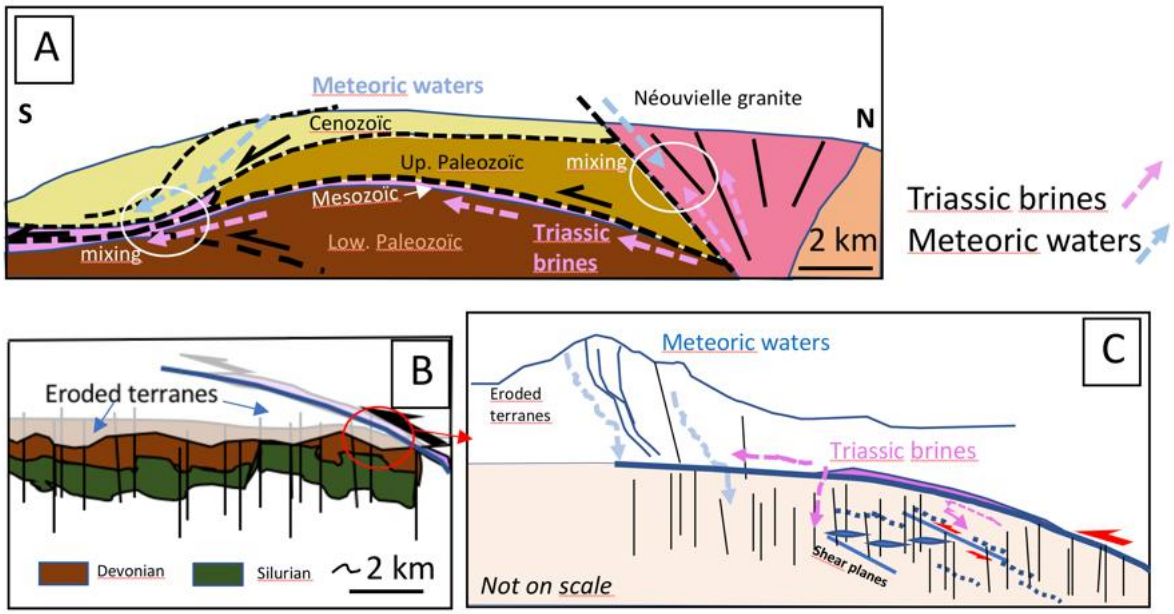

Fig. 11: Model of fluid circulation during thrusting. A- example of the Gavarnie thrust based on a cross-section slightly modified from Jolivet et al. (2007) and Trincal et al. (2015). B example, in the Ariège/ Haute Garonne area, where the Paleozoic basement characterised by a subvertical foliation, particularly Devonian marbles and quartzites are outcropping due to denudation of the overlying thrust zones. C: series of brittle structures developed close to shearing planes in the area shown in B.

Table Caption

Locality	Host-rock lithology	Geodynamic event	Mineral hosting Fis	Salinity (wt.% NaCl eq.)		Homogenization temperature(°C)		Gas (as traces)
				range	mode	range	mode	
Trimouns	Dolomite and Chlorite-micaschists	Syn - rift	Quartz (talc)	27.5-30.2	29	168 - 220	190-220	N_2-CO_2-CH_4
	Dolomite and Chlorite-micaschists		Calcite	29.3 to 33.5	29.5	166 - 226	190-220	N_2-CO_2-CH_4
Col de Jau	Querigut granite-Ordovician Paleozoic schists	Syn - rift	Quartz (talc)	30-33	30	150 - 196	160	N_2-CO_2
Reynès	Paleozoic series undifferentiated	Syn - rift	Quartz (Chlorite-talc)	27-35	29	155 - 247		CO_2-N_2 .CH_4
Vallée d'Aspe (La Cristallère)	Permian pelites/ Visean marbles	Thrust	Quartz-(albite-chlorite)	6.5-10.5	7.9	nd		
Vallée d'Aspe (Portalet)	Permian pelites or Devonian	Thrust	Quartz	8.4-11	9.2	108 - 114	110	
Estaing	Hercynian granite / Devonian marbles	Thrust	Quartz	9.2-17.9	14	176 - 236	230	
Val d'Aran	Devonian series	Thrust	Quartz	1.2-4.3	1.7	129 - 139	135	N_2- (CH_4, CO_2)
La Calabasse	Devonian- Dolomitic marbles	Thrust	Quartz-ankerite	19.3-26	23	140 - 190	175	CO2-(N2, CH4)
St Lary	Devonian- Dolomitic marbles	Thrust	Quartz	11-16.5	14	209 - 235	225	CO_2
Balacet	Devonian dolomite	Thrust	Quartz	6.9-10.5	9.2	138 - 169	135	
Couserans	Devonian dolomite	Thrust	Quartz	11.0-11.4	11.2	140 - 220		
Couledoux (Col de l'Artigascou)	Mid-Devonian dolomites	Thrust	Quartz	18-20.3	19.5	168 - 208	180	
Val d'Alet	Devonian dolomite	Thrust	Quartz	23-25	25	160 - 198	185	N_2- (CH_4, CO_2)
Mine Alzen	Devonian limestones	Thrust	Calcite	5.7-10.5	8.5	185 - 195	190	

Table 1: Overview of geological occurrences studied in this paper and related fluid inclusion data. The list includes occurrences of quartz filled tension gashes interpreted as syn-convergence, as well as syn-rift metasomatic areas.

Locality	Host-rock lithology	Geodynamic event	Mineralisation	Salinity	Salinity mode	Homogenisation temperature	Cl/Br	Traces of gas	References
				wt. % NaCl eq.	wt. % NaCl eq.	°C	(molar ratio)		
Deep Lacq	Jurassic	Syn-rift	Saddle dolomite	8 - 10	9	130-150		CH_4 - H_2S	Bahnan, 2019
Rousse	Mano dolostone	Syn - rift	Dolomite-calcite	0 - 6	3.5	145-165		CH_4-CO_2,hydrocarbons	Renard et al., 2019
Chainons Béarnais	Tithonian	Syn-rift	Dolomite DC2	0 - 3.6	1.6	170 -200			Motte et al., 2021
	Mano formation		Dolomite DC3 ab	0 - 5	1.5	150 -190			
			Dolomite DC3c	0 - 12	5	170 -200			
			Dolomite DC4	10 - 27	20	200 -320			
	Oxf-Callovian (Meillon)	Syn-rift	Dolomite DC4	13 - 24	18	240 - 260			Motte et al., 2021
			Quartz and calcite	13 - 16	14	140-220		CO_2-N_2	Salardon et al., 2016
Chainons Béarnais	Veins in Cretaceous formations	Syn - rift	Dolomite 2 core	25 - 30	30	200-260		CO_2-N_2-H_2S	
			Dolomite 2 rim	25 - 30	27	300-350		CO_2-N_2	
Urdach	Breccia Albian Cenomanian	Syn - rift	Breccia cements	10 - 23	19	200-280	2000-2300	CO_2-CH_4-N_2	Nteme Mukonzo et al., 2021
				30 - 37	34	155-200		CO_2-CH_4-N_2	
			Quartz	32 - 34	33	130-160		N_2 - CH_4 - H_2S	Corre et al., 2018
Saraille	Veins in Neocomian Aptian	Syn - rift	Calcite	15-30	20	160-220			
			Dolomite	22-27	25	180-240			
Trimouns	Siluro-Devonian micaschists and dolostones	Syn -rift	Calcite	29-33	30	130-230	300-400	CO_2-CH_4-N_2	Quesnel et al., 2019
			Dolostone-talc	21-30	25	130-230	270-360	CO_2-CH_4-N_2	
			Quartz	27-32	29	130-230	430-610	CO_2-CH_4-N_2	
Chainons Béarnais	Meillon formatiion	Post- rift	Quartz (primairy FI)	2.5 - 7.5	5.5	135 - 205			Motte et al., 2021
	Meillon formatiion	Post- rift	Quartz (secondary FI)	8 - 24	20	140 - 160			
	Meillon formatiion	Exhumation	Calcite	18	18	140 -160			
Monte Perdido	Lower Ypresian Millaris marls	Convergence stage-Thrust	Quartz and calcite	1 - 6		165-190			Lacroix et al., 2011
Gavarnie thrust									Banks et al.,1991; Mc Caig et al., 1995,2000
Gistain	Triassic red beds (close unconformity with Devonian phyllites)	Convergence stage-Thrust	Quartz barite	5 - 23	9	160-175	440 -3040		McCaig et al., 2000
Plan de Larri	Triassic red beds	Convergence stage-Thrust	Quartz	7 - 17	9	150-180	130-1000		McCaig et al., 2000
Pic Long	Neouvielle granite	Convergence stage-Thrust	Quartz	30-34	31	135-175	90-220		McCaig et al., 2000
La Glere	Neouvielle granite	Convergence stage-Thrust	Quartz	27-28	28	150-230	90-250		McCaig et al., 2000
Pic Port Vieux	Cambro-Ordovician pelites	Convergence stage-Thrust	Quartz	14-24	19	140-180	270-460		McCaig et al., 2000
Keuper	Mediano dolomites	Convergence stage-Thrust	Dolomite	31.4-32.8	32.5	115	460-480		McCaig et al., 2000
Parzan	Vein (boundary granite and Triassic)	Multistage -Mesozoic reworking	Fluorite, Zn	11 - 24	17	120-195			Fanlo et al., 1998
			Quartz	20 – 23	22	180-200			
Coll de Pal	Devonian and Cambrian carbonates	Convergence stage-Thrust ?	Barite and minor Cu sulphide	20	20	125-150			Canals et al., 1999
Upper Lacq	Albian Aptian	Convergence stage-fault	Dolomite, calcite	0 - 4	2	70-90			Bahnan et al., 2020
Deep Lacq	Triassic and Jurassic series	Post-rift (early convergence)	Calcite	9 - 14	12	100-150		CH_4 - H_2S	Bahnan, 2019
			Anhydrite	4 - 6	5	90-130			
Rousse	Campanian flysch	Convergence stage-fault	Calcite	10 - 14.5	12	155-170		CH_4-CO_2	Renard et al., 2019
Portalet	Lower carboniferous limesteones	Reworked ore deposits	Fluorite	4 - 11.5	6.5	110-200			Subias and Fernandez Nieto, 1995
Tebarray	Upper devonian marbles	Reworked ore deposits	Zn-F (Pb) Fluorite	12 -18	16	150-210			Subias and Fernandez Nieto, 1995
Lanuza	Lower devonian limestones	Reworked ore deposits	Fluorite ± calcite	14-20	16.5	140-220			Subias and Fernandez Nieto, 1995
			Pb-Zn-Ag						
Cierco	Devonian metasediment, Trias	Reworked ore deposits	Early quartz	28	28	152-173	260		Johnson et al, 1996
			Main quartz	22	21.5	150-190			
			Sphalerite	5 - 22	19	112-198	170-300		
Arre	Devonian calcschists	Reworked ore deposits	Quartz (Pb-Zn)	23-27	24.5	160-210			Cugerone, 2019
Crabioules	Late ordovician Metamorphic schists	Reworked ore deposits	Quartz (Pb-Zn)	31-39	33	220-250			Cugerone, 2019
Victoria	Late ordovician Metamorphic schists	Reworked ore deposits	Quartz (Pb-Zn)	32-38	32	220-235			Cugerone, 2019
Argut	Late Ordovician Calcschists	Reworked ore deposits	Quartz (Pb-Zn)	3-7	5.5	230-280			Cugerone, 2019
Pale de Rase	Late Ordovician Calcschists	Reworked ore deposits	Quartz (Pb-Zn)	1-10	4	200-255			Cugerone, 2019
Pale de Bideau	Late Ordovician Calcschists	Reworked ore deposits	Quartz (Pb-Zn)	5-16	15	185-320			Cugerone, 2019
Les Argentieres	Lower Devonian dolomites closed to faulted contact with Mid-Devonian calc-schists	Reworked ore deposits	Quartz (Pb-Zn)	25 -28	27	108-140			Munoz et al., 2015
Lacore	Lower Devonian dolomites closed to faulted contact with Mid-Devonian calc-schists	Reworked ore deposits	Quartz (Pb-Zn)	18 -25	22	118-180			Munoz et al., 2015

1271

Table 2: List of geological occurrences and corresponding literature on fluid inclusions for diagenetic-hydrothermal cement related to syn-rift and syn-thrust events from the Pyrenees. Data on ore deposits the most probably affected by later hydrothermal processes of unknown age were also considered.